Prediction of fracture propagation in human femur using the Finite Element Method

Frida Bengtsson

Lund, May 2018

LUND UNIVERSITY

Master's Thesis in Biomedical Engineering

Faculty of Engineering, LTH
Department of Biomedical Engineering

Supervisors: Lorenzo Grassi, Anna Gustafsson, Hanna Isaksson

Title
Prediction of fracture propagation in human femur using the Finite Element Method

Author
Frida Bengtsson

Number of pages
71

Figures
Created by the author if nothing else is indicated

Lunds Universitet
Institutionen för biomedicinsk teknik
Box 118
SE-221 00 Lund
Sverige

E-husets tryckeri
Lund 2018

Acknowledgements

I would first of all like to thank my supervisors, Lorenzo Grassi, Anna Gustafsson and Hanna Isaksson: thank you for your patience, your support and your guidance throughout this project. I have really learnt so much during this time. Thank you also to all the members of the Biomechanics group, you made this time fun and made me feel welcome from the first day.

I would also like to say a special thanks to Professor T.C. Gasser from the Royal Institute of Technology (KTH) for making his work available for us and for all the Skype-sessions where he guided me through the subroutines.

Last but definitely not least, I would like to thank my family and friends for always cheering me on and believing in me.

Contribution of the author

The concept and design of the study was planned by L. Grassi and H. Isaksson, who also provided CT-images from the two subjects used in this project as well as data from their experimental results [1]. T.C. Gasser provided the FEAP software with the PUFEM subroutines which predicts crack initiation and propagation [2].

All numerical modeling has been carried out by the author, with assistance from the project supervisors and T.C. Gasser in implementing new features. The analysis and interpretation of results has been carried out in collaboration between the author and the project supervisors. The author has written the full report, which has then been revised after suggestions by the project supervisors.

Abstract

Hip fractures constitute a major problem, both in terms of a lower life quality for the people affected and socio-economical factors. Osteoporosis is a medical condition, defined by decreased bone mass, which results in a more fragile bone structure and a higher risk for fractures. Osteoporosis accounts for a cost of €1.5 billion each year in Sweden alone, and the costs are increasing.

In order to prevent fractures from occurring, new robust methods for fracture risk assessments are needed. The majority of the computational methods available today show promising results, but do not account for the individual bone geometry or materials and are often not able to capture the complicated mechanical response of bone fractures.

In this project, a subject-specific FE modeling method was combined with a PUFEM-based code that worked on homogeneous materials. A convergence study was performed in order to find a suitable step-size in the solution method, as well as a material parameters study to confirm the accurate mechanical response of the models. The goal of the material parameter study was also to assess the influence in terms of location of fracture initiation point and fracture pathway.

At the current state, several models have been produced and tested, both homogeneous and heterogeneous models. In the homogeneous models, identical material parameters were used for cortical and trabecular bone, whereas in the heterogeneous models different stiffnesses were used for cortical and trabecular bone tissues. With these models, it was possible to calculate crack initiation and crack path as well as e.g. the stress distribution. To conclude, subject-specific FE-models showed promising result as a method to predict fractures and could lead to an improved understanding of the mechanical responses of bone.

Sammanfattning

Äldre personer drabbas ofta av lårbensfrakturer som idag utgör stora problem, både i form av stora socioekonomiska faktorer och i form av en sänkt livskvalité för de drabbade. Den årliga kostnaden för den här typen av frakturer uppskattas till €1.5 miljarder enbart i Sverige och kan därför anses som en stor påfrestning på samhället. Osteoporos, också kallat benskörhet, är en sjukdom som definieras av minskad bentäthet, vilket resulterar i en skörare benstruktur som ytterligare ökar risken för att drabbas av en fraktur.

För att förhindra att frakturer sker behövs bättre metoder för att kunna bedöma frakturrisken hos patienter. Idag finns ett flertal numeriska modeller som visar lovande resultat - de kan fånga bens mekaniska egenskaperna innan fraktur samt förutspå var och vid vilken belastning en fraktur sker. Dessa numeriska modeller kan dock i de flesta fall inte modellera längs vilken väg frakturen skulle utbreda sig, vilket hade varit fördelaktigt.

I detta projekt har patientspecifika finita elementmodeller tagits fram, där vissa element har utökats med ytterligare frihetsgrader för att kunna beskriva sprickors form och hur de propagerar genom benet (eng. partition of unity). En konvergensstudie genomfördes för att identifiera ett lämpligt steg för den iterativa process som användes för att lösa de finita elementproblemen. En materialparameterstudie genomfördes även med två syften: att bekräfta modellernas rimlighet genom att utvärdera det mekaniska beteendet vid olika värden för de olika materialparametrarna samt att undersöka materialparametrarnas påverkan på sprickbildning och sprickpropagering.

I nuläget har flera olika modeller testats och utvärderats, både homogena modeller och heterogena modeller. I de homogena modellerna

har kortikal och trabekulär benvävnad modellerats med identiska materialparametrar, medan de i de heterogena modellerna har modellerats olika. Med dessa modeller var det möjligt att förutspå både platsen för sprickbildning samt utseendet av själva frakturen. Sammanfattningsvis visade resultaten i detta projekt på stora utvecklingsmöjligheter och har potential att ge en ökad förståelse för benvävnads brottmekaniska beteende.

List of acronyms & abbreviations

δ - Displacement

δ_c - Displacement at complete separation

ε - Strain

κ - Bulk modulus

$\mathcal{G}_c$ - Fracture energy

μ - Shear modulus

ν - Poisson's ratio

σ - Stress

σ_{max} - Cohesive strength

BC - Boundary condition

BMD - Bone mineral density

CCC - Cohesive crack concept

CT - Computed tomography

DIC - Digital image correlation

DXA - Dual-energy X-ray absorptiometry

E - Young's modulus

FEAP - Finite element analysis program

FE - Finite element

HU - Hounsfield units

PUFEM - Partition of unity finite element method

SD - Standard deviation

SG - Strain gauge

Contents

Chapter 1

Introduction

Hip fractures constitute a major issue for people worldwide. In the year 1990, approximately 1.26 million people suffered from a hip fracture [3]. A study shows that due to the increasing life expectancy, the number of individuals suffering from hip fractures will increase to 4.5 million cases per year worldwide by the year 2050 [3]. The high number of fractures, and more specifically fragility fractures, i.e. fractures which occur from little trauma or impact, are both due to individual bone geometry and structure, but can also be caused by metabolic bone diseases. Osteoporosis is a condition defined by low bone mass, resulting in a fragile bone structure, which is more prone to fractures. This condition is affecting more and more people, resulting in an expected increase of costs and lower life quality for many people. Today, approximately 29% of all females and 18% of all males over 45 years suffer from osteoporosis [4, 5] and it is estimated to cost €1.5 billion each year in Sweden alone [6]. In short, fractures account for both a decrease in life quality for the people affected but also a major socio-economic effect, making it an important issue to address. By introducing a more robust fracture risk assessment or prediction, preventive measures can be taken and thereby decreasing either the occurrence or the level of severity of a fracture.

One of the current methods for assessing fracture risk is by using FRAX, an online tool which generates the 10-year risk of suffering from a fracture. FRAX includes data regarding Bone Mineral Density (BMD), a measure which is used to diagnose osteoporosis, as well as epidemiological factors such as age, gender and medical history [7]. However, it does not consider the individual bone geometry, maximum strength or specific location or path for a fracture. For that purpose, the Finite

Element Method (FEM) have been proposed as a method to include the patient-specific bone geometry and thus being able to calculate the strain, bone strength and location of fracture onset [1, 8]. Although classical FE-models have been able to accurately describe the mechanical response of a bone, they do not account for the more complicated mechanisms in bone which allow a fracture to propagate. The Partition of Unity Finite Element Method (PUFEM), an extended version of the classical FEM, has been suggested as it adds degrees of freedom to a solution, thus allowing for modeling of discontinuities and thereby capturing the fracture path [9].

1.1 Aim

The aim of this project is to use PUFEM to create subject-specific fracture predictions by including both the bone geometry and material parameters from clinical Computed Tomography (CT)-images.

1.2 Design of the study

The design of the study is as follows: clinical CT-images were used to generate subject-specific 3D-Finite element models for two human femur bones. Boundary and loading conditions were applied to resemble those defined in previous experiments [1]. The subject-specific finite element models were used to predict fracture location and pathway and the results were compared with experimental data [1].

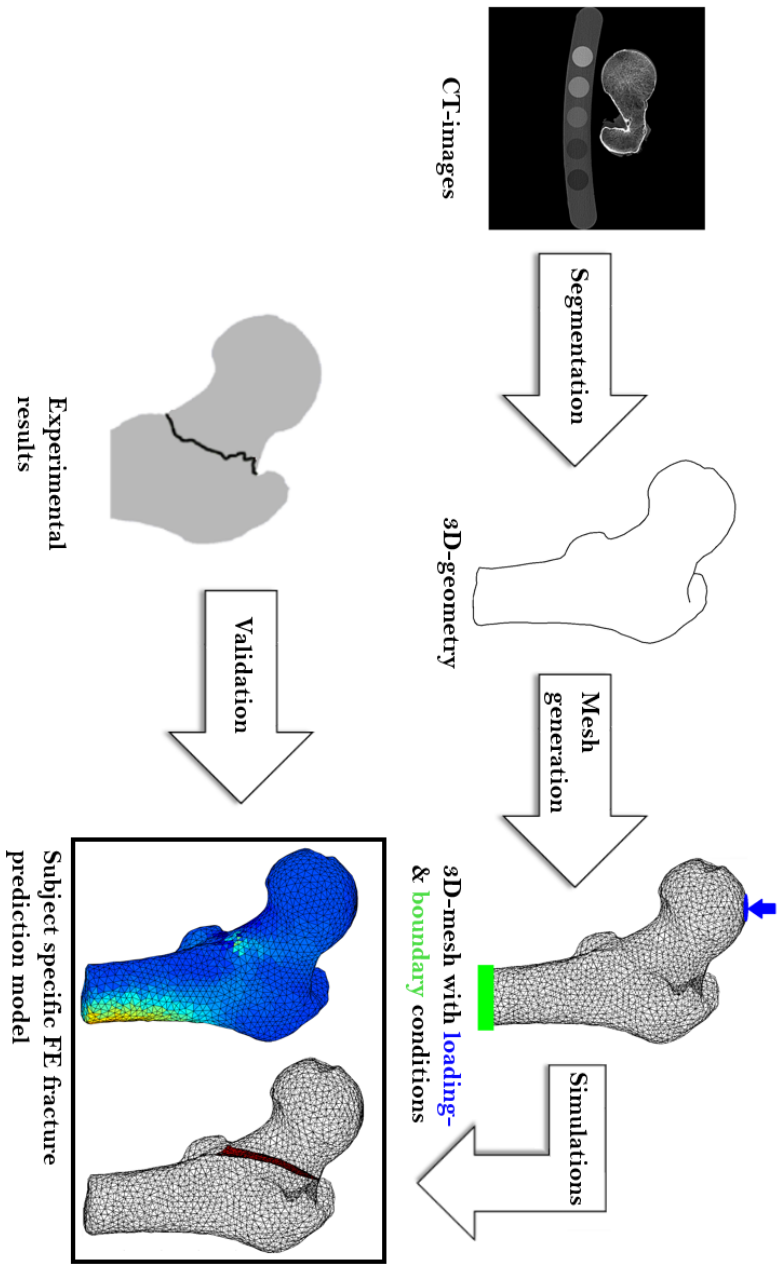

Figure 1.1: Design of the study

Chapter 2

Theory

2.1 Bone

As part of the skeletal system, bones provide support and protection, allow movement, produce blood cells and act as a storage for minerals and lipids. The human skeleton consists of 206 bones, which can be divided into several groups. One group is long bones, to which the femur, the thigh bone, belongs (see figure 2.1). The long shaft of the femur, which contains the marrow canal, is called the diaphysis. At each end, the epiphysis are located, the proximal located closest to the hip and the distal located closest to the knee. The proximal femur can be seen in more detail in figure 2.1 (b). The femoral head connects the limb to the upper body through the pelvis, and the greater and lesser trochanter are protruding areas acting as connection sites for larger ligaments and tendons. The part between the femoral head and the trochanters are referred to as the femoral neck and is the region most commonly affected by osteoporotic fractures [4].

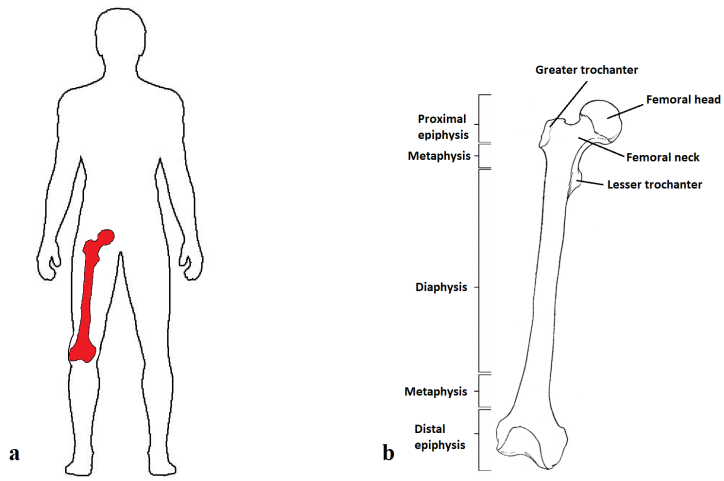

Figure 2.1: Femur - location in the human body (a) and whole bone structure (b)

In general, the long bones are built up of two types of bone tissue: compact (cortical) bone, and spongy (trabecular) bone. Both cortical and trabecular bone share the same basic composition, with cell-types called osteoblasts, osteoclasts and osteocytes. However, the two types of bones are built up from different micro-structure depending on their respective function. In the cortical bone, the osteocytes are arranged around the so-called Haversian canal, and the lamellae oriented in the same direction as the canal, i.e. along with the diaphysis of the bone. In trabecular bone, the lamellae create a network of branches, similar to a honeycomb-shape, called trabeculae (see figure 2.2). The purpose of these different structures of the bones is dependent on the functions they have. The cortical bone can, through the parallel arrangement of the lamellae and the much higher density, withstand large forces in the direction of the lamellae (along the diaphysis). However, when exposed to a sideway force in relation to the lamellae orientation in cortial bone, it can quite easily break. On the other hand, the trabecular bone is constructed in order to withstand multi-directional forces, but can in general not withstand as large forces as cortical bone [4].

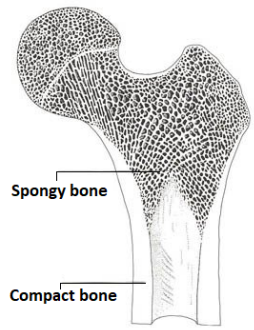

Figure 2.2: Compact and spongy bone [10]

2.2 Osteoporosis

Osteoporosis is a medical condition characterized by a decreased bone mass leading to a fragile bone structure and an increased risk of fractures. Osteoporosis can be a side-effect from another medical condition, but is generally a result of aging. The most common form of osteoporosis is therefore known as senile osteoporosis and affects most aging individuals. The normal bone loss, as an effect of aging, is an average of 0.7% bone mass decrease per year and is mostly affecting the areas which contain more trabecular bone, such as the femoral neck. These regions are therefore the location where the majority of osteoporosis related fractures occur [5].

Osteoporosis is estimated to affect 29% of all women and 18% of all men over the age of 45. Women, or more specifically, post-menopausal women, have a larger risk of suffering from fractures due to osteoporosis. This is due to the fact that after the entry of menopause, there is a decrease in certain hormones, which can accelerate the progression of bone loss [4, 5]. In the year 2010, it was estimated that osteoporosis accounted for an annual cost of €1.5 billion in Sweden alone, making it an important issue to address [6].

The current method for diagnosing osteoporosis is by measuring the bone mineral density (BMD). This is done by performing a 2D-dual-energy X-ray absorptiometry (DXA), which provides the mineral content of a bone. By dividing the mineral content by the area scanned

with the 2D-DXA, a measure of the BMD is provided. With the average BMD of a young, female reference population being $\overline{x}$, osteoporosis is then defined as a BMD $< \overline{x}$-2.5 standard deviations (SD) [11].

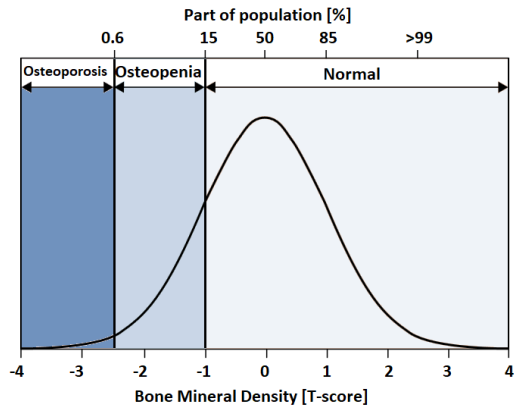

Figure 2.3: Distribution of BMD for a female population

Figure 2.3 shows the distribution of the prevalence of osteoporosis for a healthy female population and shows that approximately 15% of the population is osteopenic and 0.6% are suffering from osteoporosis [11]. Osteopenia, or low bone mass, is defined as BMD $< \overline{x} - 1$ SD but BMD $> \overline{x} - 2.5$ SD the mean and can be considered pre-osteoporosis. Values of BMD $> \overline{x} - 1$ SD below the mean can be considered a normal value.

2.3 Fracture risk assessment

To assess the fracture risk of an individual, one method is to perform a 2D-DXA, in order to get the BMD value. With this, the patient can be categorized as normal, osteopenic or osteoporotic, and if needed, potential medication can be given [12].

Another current method is an online-tool called FRAX, developed at the University of Sheffield in 2008 [7]. The purpose of FRAX is to generate a 10-year prospect regarding the risk of suffering from a fracture. The tool combines the information about BMD with clinical risk factors

such as age, sex, weight, height, smoking and alcohol habits, as well as medical history from parents.

Although the algorithms of FRAX provides promising results, there are many improvements which can be implemented in order to increase accuracy. FRAX does not include any information about the bone geometry, something which can be a significant factor in terms of fracture establishment. Some suggestions of improvement to FRAX are also to include more clinical risk factors, another is to include personalized data about the maximum load a bone can withstand without fracturing [13].

2.4 Bone mechanics

Two basic measurements in mechanical testing are stress and strain. Stress (σ) is defined as force (F) distributed over an area (A) and usually denoted as:

$$\sigma = F/A \tag{2.1}$$

with the unit N/m^2 or Pascal (Pa). Strain (ε), on the other hand, is defined as the relative deformation, i.e. the difference in length after deformation ($L_0 - L$) over the original length (L_0), or:

$$\varepsilon = (L_0 - L)/L_0 \tag{2.2}$$

(unitless). A material parameter often used in biomechanics is the stiffness. The stiffness can either be extrinsic, defined as the slope of the elastic part of a load-deformation curve, or intrinsic. The intrinsic stiffness of a material is more commonly referred to as the Young's modulus (E) and is defined as the slope of the elastic part of a stress-strain curve [14].

In order to capture the mechanical properties of bone, which is a highly complex material, several methods are available. In mechanical testing, the setups are usually equipped with a load cell which controls the force to apply on a specimen, and something to produce an output in terms of displacement [14]. Bending tests are one of the most commonly used methods to test the mechanical response of samples. A three-point bending tests is performed by placing the sample on two supports and applying a load on the top [15] (see figure 2.4 (a)). A four-point bending test is very similar to a three-point bending test but with load being

applied on two locations instead of one. By placing strain gauges (SG)s on specific locations of the sample, it is possible to capture the mechanical response in terms of strain distribution, as used in e.g. [16] (see figure 2.4 (b)). Another method which provides a mapping of the strain distribution over an entire body is to use the method of digital image correlation (DIC), further described in [1] (see figure 2.4 (c)).

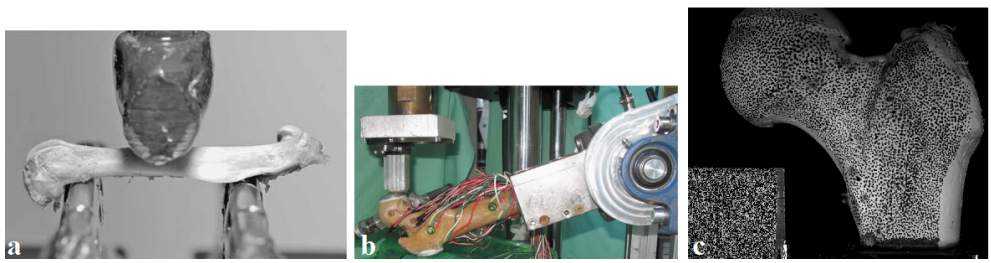

Figure 2.4: Example of methods used in bone mechanics (a) Three-point bending test [17], (b) Strain gauges [18], (c) Digital image correlation [1]. Reprinted with permission from John Wiley and Sons, Elsevier and ASME

Although these types of measurements and testing methods can provide accurate results, they all have some limitations when it comes to capture the mechanical behavior of bone. The use of SGs is highly limited by the number of SGs used and their specific location [15]. DIC could be considered an improvement to the use of SGs, since it can collect data from more points (more than 1000 points) than SGs (usually 10-15 points). However, both methods are highly time consuming and they are also limited to surface measurements.

2.4.1 Finite element bone models

The Finite Element Method (FEM) is a numerical method for approximately solving differential equations. The main objective of the method is to divide a body into a number of smaller parts, or elements, and calculations are then performed on an element level where certain approximations are made. One common approximation to be made is that a variable varies linearly in an element, even though it shows a typical non-linear behavior over the total body. By thereafter assembling the results from each element, the FEM can achieve an approximated result

of the behavior of the entire body.

The simplicity of this method makes the FEM applicable on a variety of problems, for example heat conduction, fluid problems, torsion, bending etc. For a more detailed description of the underlying mathematics of FEM, the reader is referred to [19]. In recent years, the development of FE programs has evolved with increasing computational power and a number of softwares are available in order to solve non-linear, transient, partial differential equations [20].

A number of researchers have been using the FEM to model the mechanical behavior of bones, without making the models subject-specific, among them e.g. [2]. However, a subject-specific model would presumably produce more accurate results since the e.g. strength of a bone is highly dependent of the bone geometry and the individual material properties. One of the first to use the FEM to predict fractures in bones, based on the subjects themselves, was J.C. Lotz et. al. [21]. They used CT-images from two cadaver femora in order to capture the geometry of the proximal femur as well as material parameters and simulated a single-leg-stance and a lateral fall. The results from the models, stress distributions mapped over the entire geometry, were used to compare the predicted data to in vitro measurements from SGs and failure loads [21]. Since J.C. Lotz et. al., several others have produced more elaborate models and to use FEM in biomechanics is a continuously growing area.

However, even though there are a number of models accurately describing the biomechanical behavior of bones in terms of strain and stress distribution [1, 21] they do not include information about crack propagation or fracture.

2.4.2 Finite element modeling of fractures in bone

In order to model discontinuities, such as a crack in a material, one method is to continuously update the mesh, by making refinements or completely remaking the mesh, to fit the new geometry following the discontinuities. To avoid the need of continuously update the mesh, other methods were developed. In 1996, J.M. Melenk and I. Babuska described the theory and possible fields of application for the Partition of Unity Finite Element Method (PUFEM) [22]. The PUFEM is

an further developed version of FEM based on the Partition of Unity, which enhances the solution space, making it possible to also handle differential equations with strong discontinuities. By adding additional degrees of freedom to certain nodes, it allows a discontinuity, such as a crack, to take form while also avoiding re-meshing completely [23]. For a more detailed description of the underlying mathematics of PUFEM, the reader is referred to section 2.5 and [22].

The introduction of PUFEM made it possible for further development of biomechanical modeling, where discontinuities such as cracks and fractures could be mathematically described. With PUFEM, the models could be used to produce the same output as using the standard FEM, i.e. e.g. stress and strain distributions, but in addition to this also parameters such as fracture energy and more accurate descriptions of crack paths and initiation. However, one downside of PUFEM in comparison to the standard FEM is the need of larger computational power and storage space.

2.5 PUFEM

A crack or failure of any material can be seen as a discontinuity in the displacement or strain field and can be described using the strong discontinuity approach. Assuming a body $\partial\Omega_0$ exists and that a discontinuity $\partial\Omega_{0d}$ separates this body into sub-bodies which occupy the sub-domains $\partial\Omega_{0+}$ and $\partial\Omega_{0-}$. A deformation $\mathcal{X}$ maps the sub-domains $\partial\Omega_{0+}$ and $\partial\Omega_{0-}$ into their relative configurations $\partial\Omega_+$ and $\partial\Omega_-$ (see figure 2.5). With $\mathbf{X}$ being a material point, the resulting jump in the displacement field can be written as

$$u(X) = u_c(X) + \mathcal{H}(X)u_e(X) \tag{2.3}$$

where u_c and u_e are the regular and enhanced displacement field, respectively [2]. Furthermore, $\mathcal{H}$ represents the *Heaviside* function and takes the values 0 for $\partial\Omega_-$ and 1 for $\partial\Omega_+$. This means, that for $\partial\Omega_-$, the displacement of the material point $\mathbf{X}$ can be written as

$$u_- = u_c(X) + 0 \cdot u_e(X) = u_c(X) \tag{2.4}$$

and for $\partial\Omega_+$

$$u_+ = u_c(X) + 1 \cdot u_e(X) = u_c(X) + u_e(X) \tag{2.5}$$

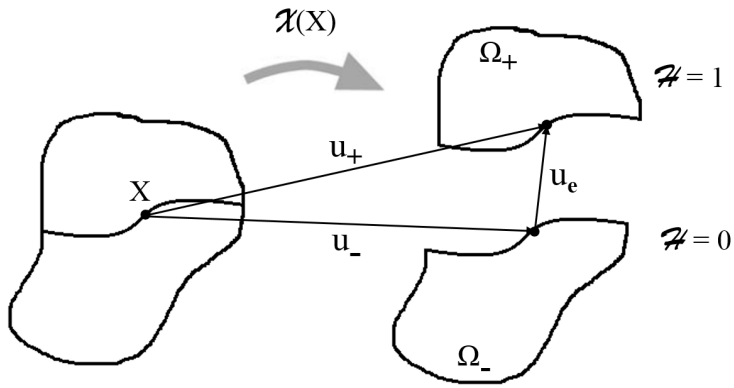

Figure 2.5: Strong discontinuity kinematics capturing a crack

In PUFEM, where the partition of unity is used, the general displacement field $\underline{u}$ can be written as

$$\underline{u} = \sum_{i=1}^{n_{elem}} N^I \underline{u}_{Ic} + \mathcal{H} \sum_{i=1}^{n_{elem}} N^I \underline{u}_{Ie}, \tag{2.6}$$

where N^I are the finite element shape functions, n_{elem} the number of nodes per element, $\mathcal{H}$ the *Heaviside* function and $\underline{u}_{Ic}$ and $\underline{u}_{Ie}$ are the regular and enhanced nodal displacements, respectively.

2.5.1 Cohesive crack concept

The cohesive crack concept (CCC) or cohesive zone model is a model in which a fracture is assumed to be a gradual process where surfaces separate from each other. The separation of surfaces is resisted by a cohesive traction, and the stress (σ) will therefore first increase with increasing surface displacement (δ) until a certain threshold called the cohesive strength (σ_{max}) is reached. Thereafter, the stress decreases to zero at the displacement at complete separation (δ_c), i.e. at the displacement where an open crack of the material, occurs [24]. An integration of the function described in figure 2.6, i.e. the area under the graph, is equivalent to the fracture energy. The fracture energy ($\mathcal{G}_c$) is the energy needed in order to achieve the separation of surfaces, i.e. to open the crack. The CCC is implemented in the present work to model a fracture in bone [2].

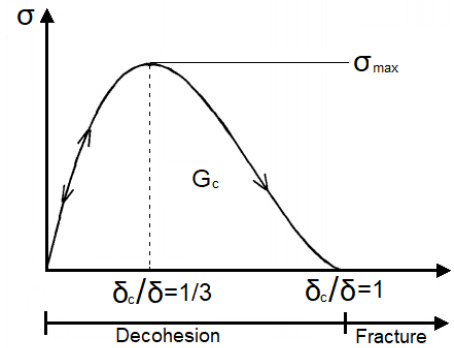

Figure 2.6: Cohesive Crack Concept

2.5.2 Fracture initiation criterion

In order to model crack or fracture initiation, a non-local version of the so-called Rankine Criterion can be used. The Rankine Criterion says that failure occurs when the maximum principal stress in an element exceeds a predefined threshold, in this case the cohesive strength (σ_{max}). The *non-local* Rankine criterion is based on the average stress, computed in a sphere with some determined radius. The element, located in the center of the sphere, is defined as cracked if the maximum principal stress in the sphere exceeds the cohesive strength (σ_{max}). The orientation of the crack is defined as perpendicular, i.e. the normal vector (N), to the direction of the maximum principal stress.

To use a non-local fracture criteria can be considered an advantage to a local criteria since the appearing of cracks due to very local stress concentrations can be avoided. Another advantage is that the fracture initiation criterion becomes less mesh-dependent. By always averaging over a pre-determined volume, and not one element, which can vary in size, the results would be more consistent for different mesh sizes. Important to note is that the fracture initiation criterion only gives information about the geometry of the crack, i.e. the propagated crack path, and does not describe whether the crack has exceeded the energy needed for a complete separation of materials, i.e. a crack opening [2, 25].

2.5.3 Two-step predictor-corrector algorithm

In order to track a crack propagation, a two-step predictor-corrector algorithm has been proposed. As the name suggests, the algorithm consists in short of two main steps: the first one is to predict the crack's propagation according to the fracture initiation, i.e. which elements have exceeded the criterion formulated above and therefore have potential to fail, and the crack tip data. The crack tip data can be described by the tip-point (P_t) and the tip-facet, as shown for the 2D-case in figure 2.7.

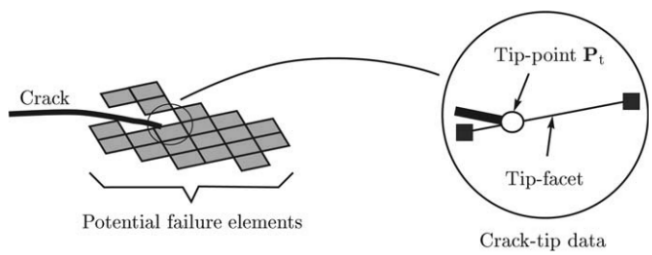

Figure 2.7: Crack surface in 2D [9]. Reprinted with permission from Elsevier

In 3D, the crack-tip data, i.e. the discontinuities, can be described by surfaces in shape of triangles or quadrilaterals. The triangles, or quadrilaterals, can be uniquely described by the point $\mathbf{P}$, determined by the crack front and located inside the discontinuity, and the normal vector $\mathbf{N}$, determined by the direction of the maximum principal stress. As the predefined criterion is met by more and more elements, the crack will propagate through the material.

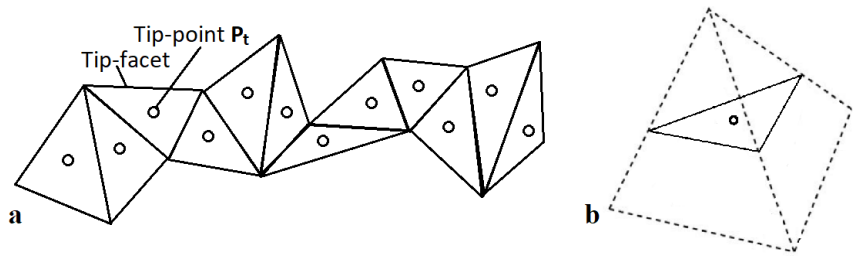

Figure 2.8: Crack surface (a) and crack surface within one tetrahedral element (b)

In some situations, the discontinuity predicted by the algorithm, may not conform well with the existing crack and may lead to crack formations which do not appear in real life. Such a situation is shown in figure 2.9 (a) and (b) where the surface in (b) clearly does not fit in with the surrounding crack surfaces. The second step of the algorithm, the corrector-step, therefore fits a new surface with the new normal vector N^* to the crack path surrounding the discontinuity surface (figure 2.9 (c)), allowing for a smoother crack path [9].

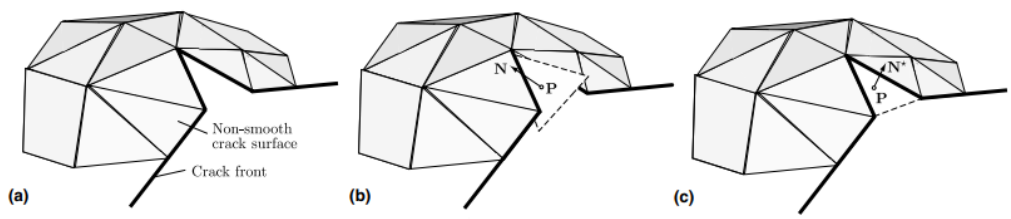

Figure 2.9: The corrector-step of the two-step algorithm [9]. Reprinted with permission from Elsevier

2.5.4 Solution methods

To solve a finite element problem, equilibrium iterations can be performed. The Newton-Raphson method both checks that the current solution is at equilibrium, within some error margin, and if not, it performs iterations and in each step, corrects the solutions to meet the desired accuracy. The equilibrium equation can be written as

$$r(u, f) = f - g(u) = 0 \tag{2.7}$$

where the the residual force $r(u, f)$ is the difference between external, f, and internal, $g(u)$, forces, respectively. In complete equilibrium, the residual force would be equal to zero [26].

To solve the present finite element problem, a special case of the arc-length method is used. A pre-defined displacement, a length, is set for each step in the solution to a control node (see values in table 3.3). For each step and displacement, the applied load is estimated accordingly to meet equilibrium. If equilibrium is not met at the initial estimate of the load, iterations with new estimates of the load are performed until the absolute value of the residual force is smaller than the predefined tolerance.

2.6 Background research for this project

This Master's thesis is based on previous work from two research groups [1, 8, 2]. Their work will be summarized in the sections below.

Grassi et al. performed mechanical tests to simulate a single leg stance with loading of the femur head until fracture. They used high-speed camera recordings and DIC to obtain a full-field displacement map over the proximal femur during mechanical tests for three human femurs. The femurs were cut approximately 5.5 cm below the lesser trochanter, and thereafter placed into a steel pot and fixated with a cold-cured epoxy-resin. A sketch of the experimental set up can be seen in figure 2.10 [1]. Not only could the results obtained in this study be used as a more accurate representation of the displacement field, the results could also be used as validation for subject-specific FE models [8].

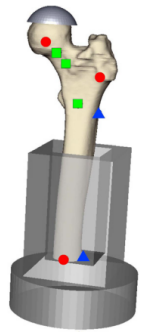

Figure 2.10: Sketch of the experimental setup in [1]

Grassi et al. extended their work to construct subject-specific FE models for the femur specimens [8]. By obtaining the geometry for each femur through a segmentation of clinical CT-images, a subject-specific mesh and FE model could be produced. The mesh had approximately 100 000 tetrahedral elements and mechanical properties was modeled according to the Hounsfield units (HU)-values from CT-images. By modeling the same scenario as in [1], loading of the femur head up to fracture in a single leg stance, the results from [1] could be used as a validation of the FE-predicted strains. The material model implemented was a modified linear elastic model. In short, a material was given a specific Young's modulus which, when exceeding a predefined threshold for yield strain (ε_y), decreased to 5.5% of the tangent modulus. The element was defined as fractured when another threshold, the ultimate strain limit (ε_f), was exceeded (see figure 2.11) [8].

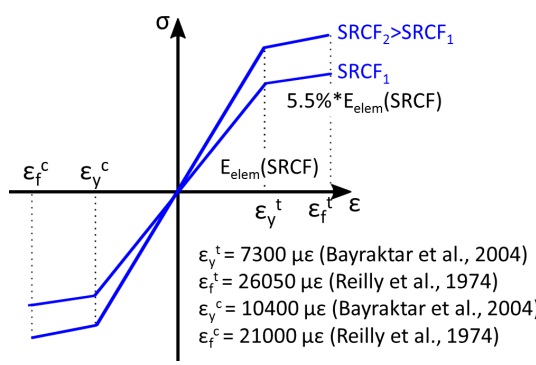

Figure 2.11: Material model used in [8]. Reprinted with permission from Elsevier

In 2007, Gasser and Holzapfel suggested using PUFEM, in order to model model fracture mechanical behavior of femur bone [2]. They combined the cohesive crack concept and the two-step predictor-corrector algorithm (see sections 2.5.1 and 2.5.3) in order to model a crack propagation. Their model included a mesh of approximately 25 000 tetrahedral elements and modeled the entire femur as a homogeneous material. The study used the geometry from a standardized proximal femur. The FE model was loaded on the femoral head, simulating a single leg stance, and were able to achieve results of bone failure comparable to experimental data in literature. Gasser and Holzapfel used a Neo-Hookean material model with the following strain-energy function:

$$\Psi = \kappa(ln(J))^2/2 + \mu(I : \overline{C} - 3)/2 \tag{2.8}$$

where κ is the bulk modulus, J is the determinant of the deformation gradient tensor, μ is the shear modulus, I the unit matrix, and $\overline{C}$ the right Cauchy Green deformation tensor.

In a Neo-Hookean material model, for given values of Young's modulus and Poisson's ratio, the bulk and shear modulus can be described with the following equations:

$$\kappa = \frac{E}{3(1-2\nu)} \tag{2.9}$$

$$\mu = \frac{E}{2(1+\nu)} \tag{2.10}$$

where E is the Young's modulus, ν the Poisson's ration, κ the bulk modulus and μ the shear modulus.

In table 2.1 below, a comparison of [8] and [2] can be found. The purpose of the comparison was to capture the advantages with both approaches, and to create a FE-model which included the majority of these.

Table 2.1: Comparison of Grassi et. al. [8] and Gasser and Holzapfel [2]

Advantage	**Grassi et. al. (2014, 2016)**	**Gasser, Holzapfel (2007)**
Fine mesh	x	
Heterogeneous material	x	
Subject-specific models	x	
Fracture initiation	x	x
Fracture propagation		x
Validation against experimental data	x	

Chapter 3

Materials & methods

3.1 Material

CT-images from two male human femurs were used in this project. The CT-images were obtained from Grassi et al. [1]. The data for the samples used can be observed in table 3.1.

Table 3.1: Sample data [1]

Sample	Age (yr)	Height (cm)	Weight (kg)	Side (L/R)
1	58	183	85	R
2	58	183	112	L

Both specimens were obtained through an ethically approved protocol (ethical permission by National Authority for Medicolegal Affairs 5783/2004/044/07) [1].

3.2 Segmentation of CT images

In order to obtain the three-dimensional geometry of the femurs, segmentation of the CT-images was performed in the software Stradwin (Version 5.3, Medical Research Imaging Group, Cambridge University Engineering Department). Stradwin uses a semi-automatic segmentation method including thresholding to collect the three-dimensional outer shape of the femurs. Stradwin also allows for a mapping of the thickness of cortical bone using the HU-values as described by Treece et

al. in [27]. A screen-shot from the program Stradwin can be observed in figure 3.1 below.

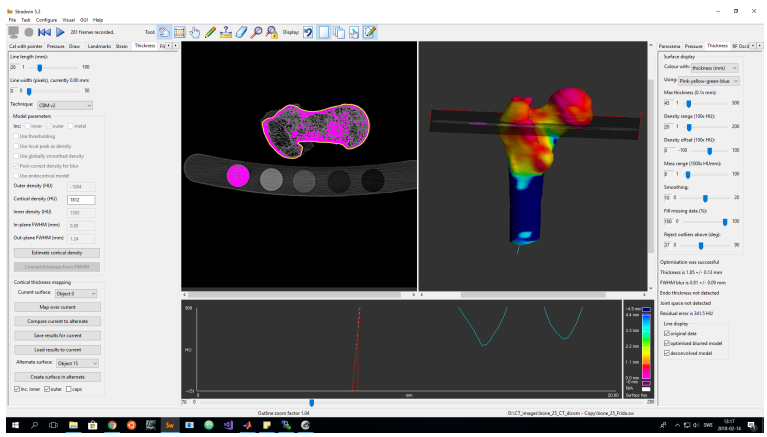

Figure 3.1: Segmentation and mapping of cortical thickness in Stradwin

3.3 Mesh generation

The first step of the mesh generation was made in Matlab (Version R2016a, Math Works, Natick, NA, USA) where the outer geometry of the femur samples was projected according to the cortical thickness, here represented as a vector, to produce an inner geometry. After that, the inner and outer surfaces were controlled and repaired in order to avoid overlapping segments and holes. The surfaces were then used as input to the software Altair Hypermesh (Version 2017, Altair Engineering Inc., Troy, MI, USA), where a finite element mesh consisting of tetrahedral elements could be generated for each femur geometry. The purpose of using both an outer and an inner geometry is to allow separate modeling of the cortical and trabecular bone, i.e. to represent them with different material properties.

3.3.1 Coordinate system

In order to be consistent in the alignment of the femur specimens, a coordinate system corresponding to that of the experimental setup in [1] was used. Pre-calculated transformation matrices, specific for each bone specimen [1], were obtained and applied to the generated nodes

resulting from the mesh generation, resulting in the rotation visible in figure 3.2.

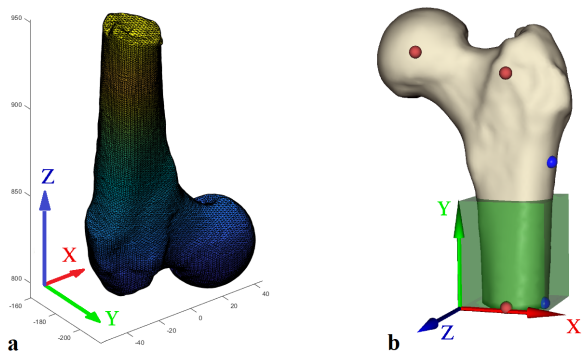

Figure 3.2: Transformation of coordinate system, (a) before, (b) after. Reprinted with permission from Elsevier [13]

3.4 Finite element models

3.4.1 Material model and material parameters

A Neo-Hookean material was used to model the bone tissue as described in 2.6.

The modeled material was assigned the following parameter values, according to those used in [2], which for the following simulations can be seen as the "baseline" values:

Table 3.2: Material parameters assigned to the finite element model [2]

Material parameter	**Value**
Young's modulus (E)	10 GPa
Poisson's ratio (ν)	0.35
Bulk modulus (κ)	11.1 GPa
Shear modulus (μ)	3.7 GPa
Cohesive strength (σ_{max})	7.0 MPa
Fracture energy ($\mathcal{G}_c$)	2.0 kJ/m^2

3.4.2 Material limits

The first model produced contained two materials, with the purpose of later being able to separately describing the cortical bone and one describe the trabecular bone. However, at this stage, the two materials were modeled with the same material parameters, i.e. the model was homogeneous.

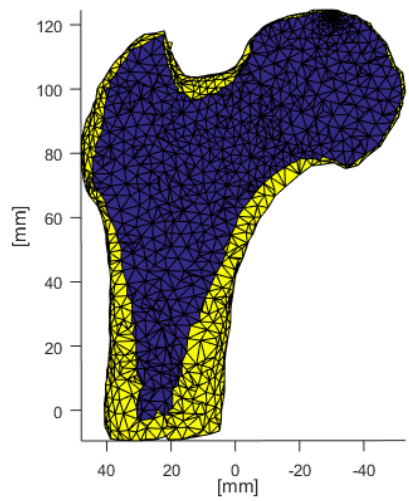

Figure 3.3: Mesh for sample 2 with 2 materials

To avoid crack formation in the distal region of the femur, a model with a dividing line below the lesser trochanter was also generated. The purpose of the dividing line was to be able to define that only the upper material(s) were allowed to crack. The use of both a horizontal and a tilted line was investigated. The horizontal line was introduced to avoid crack formation in the proximity of the boundary conditions (BC)s (see section 3.4.3) and the tilted material line in order to avoid crack formation due to bending in the lateral part of the shaft. Models with both three and four materials were tested. The models with three materials were homogeneous (with the same material parameters in all materials), and the models with four materials could either be homogeneous or heterogeneous (different material parameters for cortical and trabecular bone, respectively).

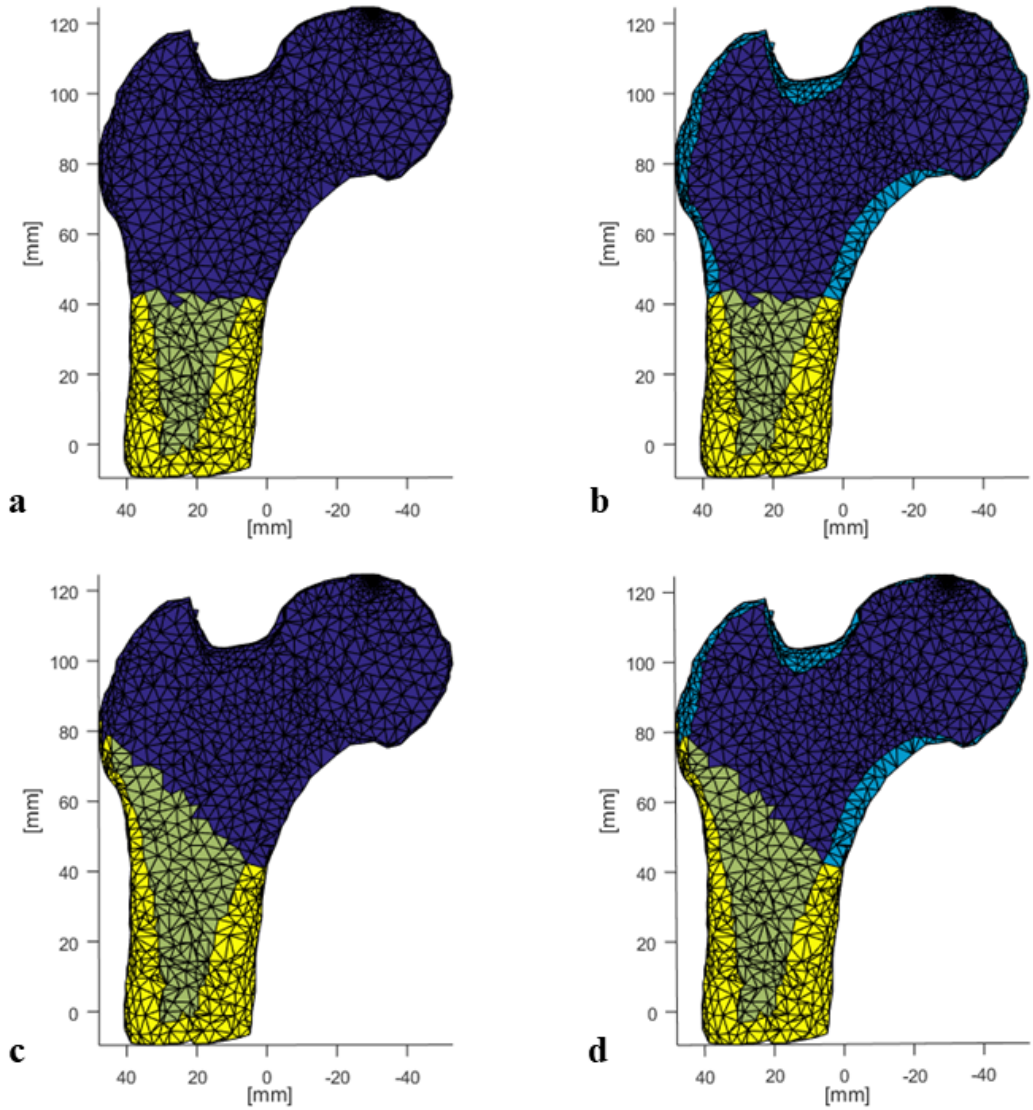

Figure 3.4: Mesh for sample 2, (a) horizontal line, 3 materials, (b) horizontal line, 4 materials, (c) tilted line, 3 materials, (d) tilted line, 4 materials

The meshes which were used for the final simulations were the following (all with a tilted material line):

- three materials (homogeneous model), figure 3.4 (c)
- four materials (homogeneous model), figure 3.4 (d)
- four materials (heterogeneous model), figure 3.4 (d)

The purpose of having two homogeneous models, one with three and one with four materials, is to test the stability of the fracture initiation criterion and two-step algorithm. The subroutines which implemented these features did allow for multiple materials in a model, but a crack could only form and propagate within the same material. That meant that certain alterations of the subroutines had to be made in order to allow the crack to move from one material model to another. To confirm the stability of the new subroutines, the result of the homogeneous model with four materials were compared to those of the homogeneous model with three materials. The reason for having three materials in one of the homogeneous models, and not only two, is simply to avoid re-segmentation. The initial model produced after segmentation consisted of two materials, resulting in a model of four materials after the introduction of a material line. It was therefore easier to only convert the upper part into one material than to remake the initial model. Naturally, the lower part could also have been made into one material, but since it was not the region of interest in this project, it was not considered necessary.

3.4.3 Boundary conditions

Boundary conditions were applied by fixating all nodes located at the most distal part of the femoral shaft in the x- and z-directions (green in figure 3.5) and two additional nodes fixated in all directions (x, y, z) (red in figure 3.5).

Forces were applied on the femoral head over a region corresponding to the area used in the experiment of [1], i.e. over the most superior nodes of the femoral head (blue in figure 3.5). According to the arc-length method as described in 2.5.4, the load was applied in steps, or iterations. Due to limitations of the software, it was at the current time only possible to perform 1 000 iterations.

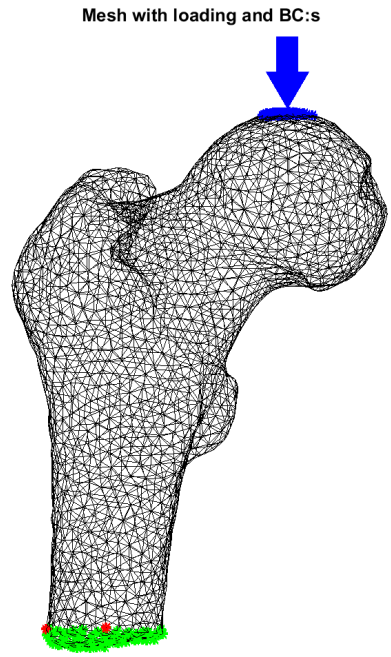

Figure 3.5: Illustration of boundary conditions, sample 1

3.5 Simulations

The simulations were performed using the solution method described in section 2.5.4. The control node used to apply the prescribed displacement were located on the lateral femoral head.

3.5.1 Software

In this project, the FEAP-software [28] was used in order to model subject-specific initiation and propagation of fractures in femur when subjected to loading. Specifically, the subroutines written by Gasser and Holzapfel which implemented the fracture initiation criterion and the fracture propagation algorithm (see sections 2.5.2 and 2.5.3) in the FEAP software were used in this project.

3.5.2 Convergence study

In order to determine the appropriate step-size, i.e. displacement, for the arc-length solution method, a convergence study was performed.

For the study, the 2^{nd} bone sample was used and the study was performed on the models with a tilted material line (homogeneous models with both three and four materials, figure 3.4 (c) and (d)), with boundary conditions applied on the distal part of the shaft (as described in 3.4.2 and 3.4.3). By continuously decreasing the step-size, and recording the location, force and displacement of the crack initiation, as well as maximum force and displacement, i.e. at crack opening, a comparison could be done. The step-sizes tested, all in the negative direction of the y-axis, can be seen in table 3.3 below.

Table 3.3: Displacement step-sizes tested in convergence study

Displacement [mm]
-0.2
-0.1
-0.05
-0.025
-0.0125
-0.005
-0.001
-0.0005

3.5.3 Material parameter study

In order to validate the FE-models in terms of accurate mechanical response, a material parameter study was performed. The purpose was also to test the influence varying material parameters had on fracture initiation and pathway.

For the material parameter study, the mesh of bone sample 1 was selected and used. The material line used was tilted and the simulations were performed on both the homogeneous and heterogeneous models with three and four materials, and the boundary conditions were as described in 3.4.3 and figure 3.5.

Cohesive strength

Simulations were performed on the meshes with varying values of the cohesive strength (σ_{max}) and the other parameters remaining as the baseline values (see table 3.2). The values tested can be seen in table 3.4 below and are based on values from [29, 30, 31].

Table 3.4: Values of cohesive strength tested in material parameter study

Cohesive strength (σ_{max})
7 MPa
20 MPa
50 MPa
100 MPa

Stiffness

Simulations were then performed with varying values of the Young's modulus (E). First, the entire bone was modeled as homogeneous, i.e. all materials had the same material parameters, and the Young's modulus varied according to the values in table 3.5a. The resulting values of bulk and shear moduli according to equation 2.9 and 2.10 are also noted. Thereafter, the value of all material parameters of the cortical bone was fixed at the baseline level (see table 3.2), and the values of the Young's modulus of the trabecular bone varied according to the values in table 3.5b. The variation of the values for the homogeneous values are based on the baseline values from [2] and results from [32]. The values for the trabecular bone material are based on the maximum and minimum values presented in [33].

Table 3.5: Values of Young's modulus tested in material parameter study

(a) Homogeneous model (three and four materials)

Homogeneous model			
E **[GPa]**	ν	κ **[GPa]**	μ **[GPa]**
5	0.35	6	2
10	0.35	11	4
20	0.35	22	7
30	0.35	33	11

(b) Heterogeneous model

Heterogeneous model			
E **[MPa]**	ν	κ **[MPa]**	μ **[MPa]**
250	0.35	278	93
750	0.35	833	278
1000	0.35	1111	370
3000	0.35	3333	1111

Chapter 4

Results

4.1 Convergence study

The results from the convergence study regarding the step-size to be used in the arc-length method can be visualized below. Figure 4.1 shows the distance between the crack initiation point for each value and the crack initiation point for the smallest step-size. In figure 4.1, the values appear to have stabilized for the three smallest step-sizes, and no major shift in crack initiation point can be seen. The entire convergence study was performed on sample 2, both three and four homogeneous materials, with the material parameters as those defined as baseline values (see table 3.2). The difference in the results between the models with three and four materials can be explained by the different averaging methods which occurs when the crack formation is in the proximity of a material line (see section 2.5.2 and 5.1 for more details).

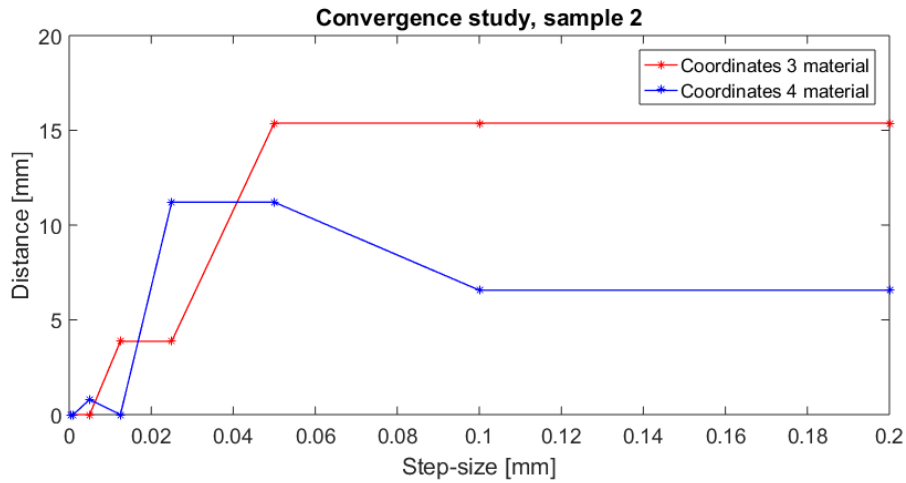

Figure 4.1: Results from convergence study, crack initiation point (in relation to the crack initiation point of the smallest step-size, 0.0005 mm) vs. step-size, sample 2

The crack initiation points as a function of step-size can also be visualized in relation to the femoral geometry in the figure 4.2 below. For visual purposes, the element marked in the figure is the first element *at the bone surface* to crack.

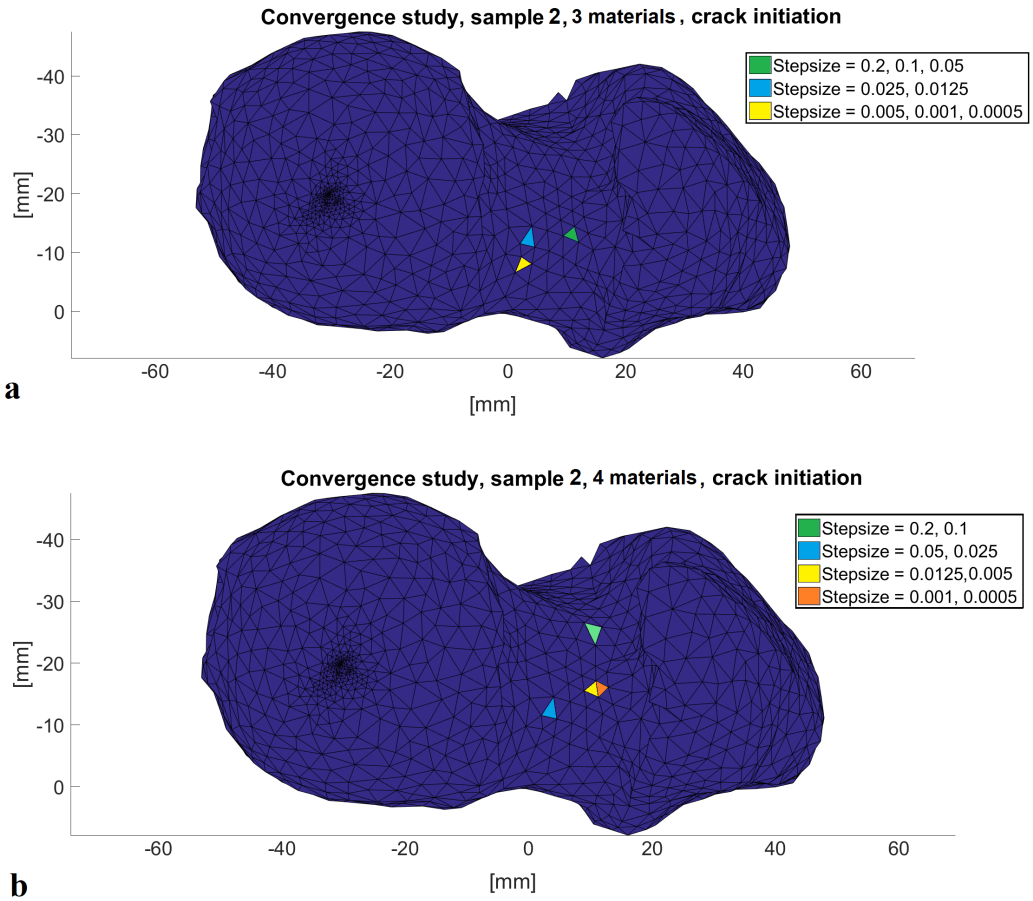

Figure 4.2: Crack initiation point, sample 2, with (a) 3 materials, (b) 4 materials

The force-displacement curves for the models tested displayed similar behavior with an initial phase of a more or less linear curve with positive slope, followed by a sudden drop in the force. The point of the drop indicated the crack opening, i.e. the maximum force the bone model can withstand before cracking completely and the displacement at that time. The following figure, figure 4.3, shows a representative example of a force-displacement curve for sample 2, modeled with three homogeneous materials. In the force-displacement curve, crack initiation and crack opening are indicated. In the current implementation, the subroutines do not allow to get accurate information about fracture

energy, i.e. when the crack actually opens. What is denoted as crack opening in the figures below, is the maximum force, used as an indication of crack opening based on similar behavior for existing data [1, 2]. The part of the plot in figure 4.3 which follows the drop, should be considered with caution. This part indicates a recovery phase after a crack opening. The increasing values indicates that there is still some parts in the structure which can bear load, for continuously increasing force. This is something which would not appear in real life and the values after crack opening have therefore not been included in any analysis.

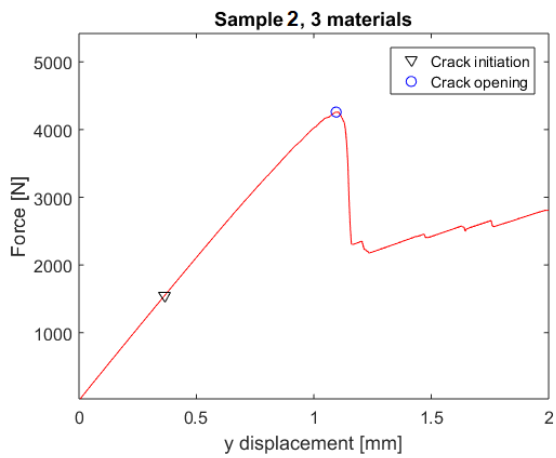

Figure 4.3: Example of a force-displacement curve, sample 2, with 3 materials

Figure 4.4 shows the result of the registered forces at crack initiation and maximum force recorded, i.e. crack opening, in relation to varying step-sizes. The force is recorded at the nodes where the load is applied with load, i.e. the most superior nodes at the femoral head.

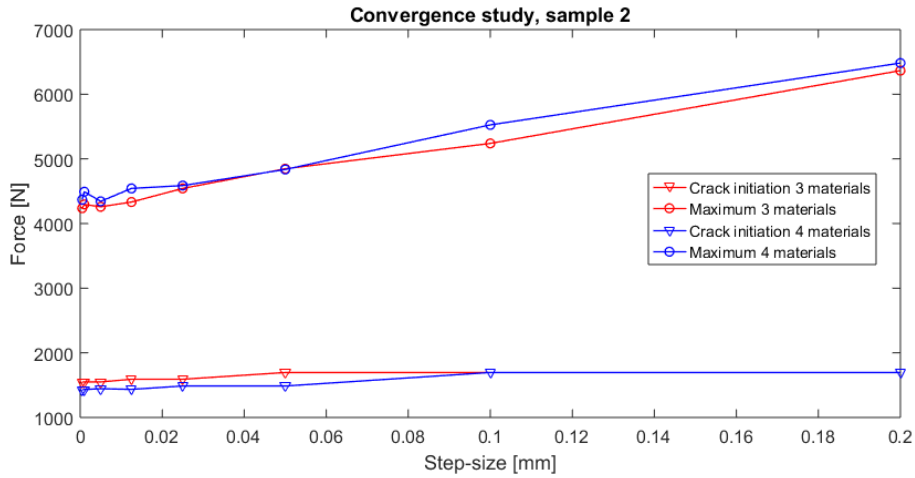

Figure 4.4: Results from convergence study, force vs. step-size, sample 2 (homogeneous models)

The results in figure 4.4 show a very similar behavior for the two models, i.e. there is a small difference in resulting force between the two. It can also be noted that the force required for crack initiation is close to unaffected by varying step-size. The step-size has however a much larger impact on the maximum force recorded. From these results, it was concluded that a step-size of 0.005 mm would be the most appropriate to use. Further reductions of the step-size did not results in significant changes in the predictions (see table 4.1).

Table 4.1: Convergence study, force at crack opening and force at crack initiation for step-sizes 0.005 and 0.0005 mm

	Crack initiation [N]		**Crack opening [N]**	
Step-size	3 materials	4 materials	3 materials	4 materials
0.005	1550	1445	4259	4343
0.0005	1548	1430	4238	4368
Difference	-0.13%	-1.05%	-0.50%	+0.57%

4.2 Material parameter study

4.2.1 Baseline model

In figure 4.5 and 4.6 below, the crack formation and maximum principal stresses can be visualized. The results are from sample 1, homogeneous with four materials, with the material parameters assigned as the baseline values. Each sub-figure shows one step in the solution, marked in the caption with the current displacement applied to the control node used in the arc-length method. As the crack propagates through the femoral neck (figure 4.5), a stress concentration clearly follows the crack tip-point (figure 4.6). A larger stress concentration can also be seen at the lateral shaft which proves the purpose of the material line. For a better visual representation of the stress, the stresses of the nodes applied with load, have been set to zero.

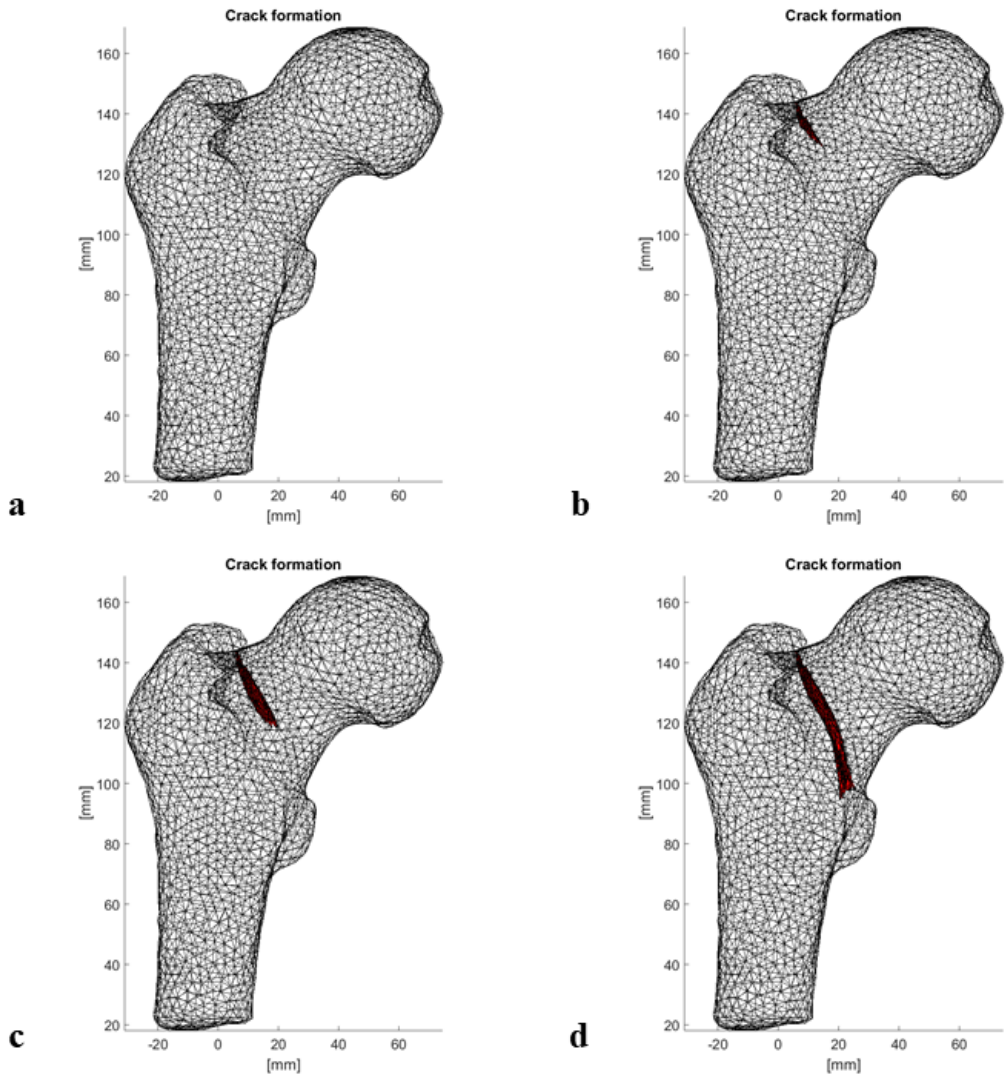

Figure 4.5: Progression of crack formation, sample 1, 4 materials (homogeneous) at displacement (a) 0.505 mm, (b) 1.005 mm, (c) 1.505 mm, (d) 2.005 mm

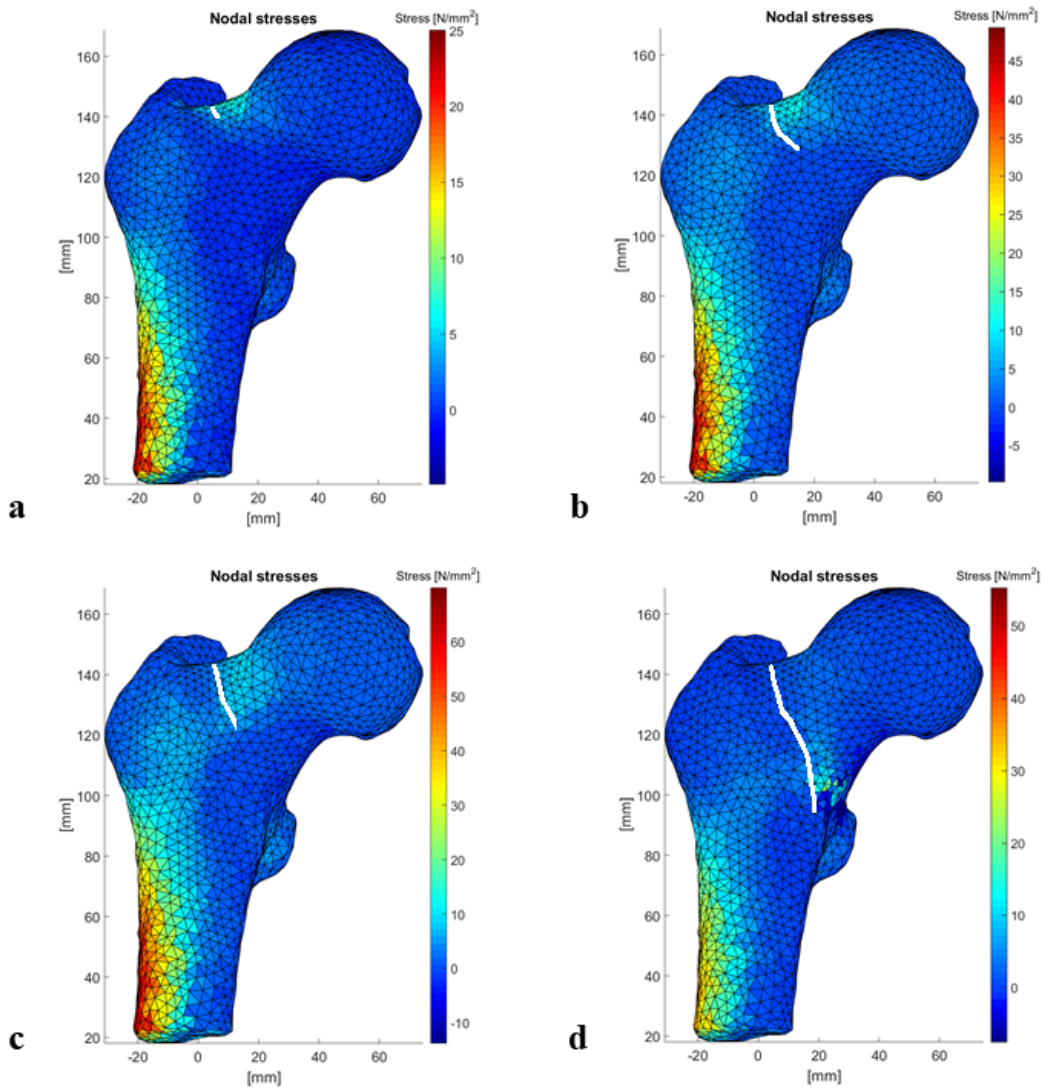

Figure 4.6: Progression of maximum principal stresses (with crack progression superimposed), sample 1, 4 materials (homogeneous), at displacement (a) 0.505 mm, (b) 1.005 mm, (c) 1.505 mm, (d) 2.005 mm

In figure 4.7 below, the maximum principal stresses, crack formation, nodal displacements (enhanced by a factor 5 for clarifying purposes) and a plot of the elements cracked can be visualized. The prolongation of elements in the femoral neck in figure 4.7 (c) of nodal displacement represents the location of the opened crack but gives the appearance of the material being stretched. The images in figure 4.7 are from the

final step of the simulation (at a displacement of 5 mm) and for the same sample as described above, i.e. sample 1, with four materials (homogeneous) and baseline values for the material parameters.

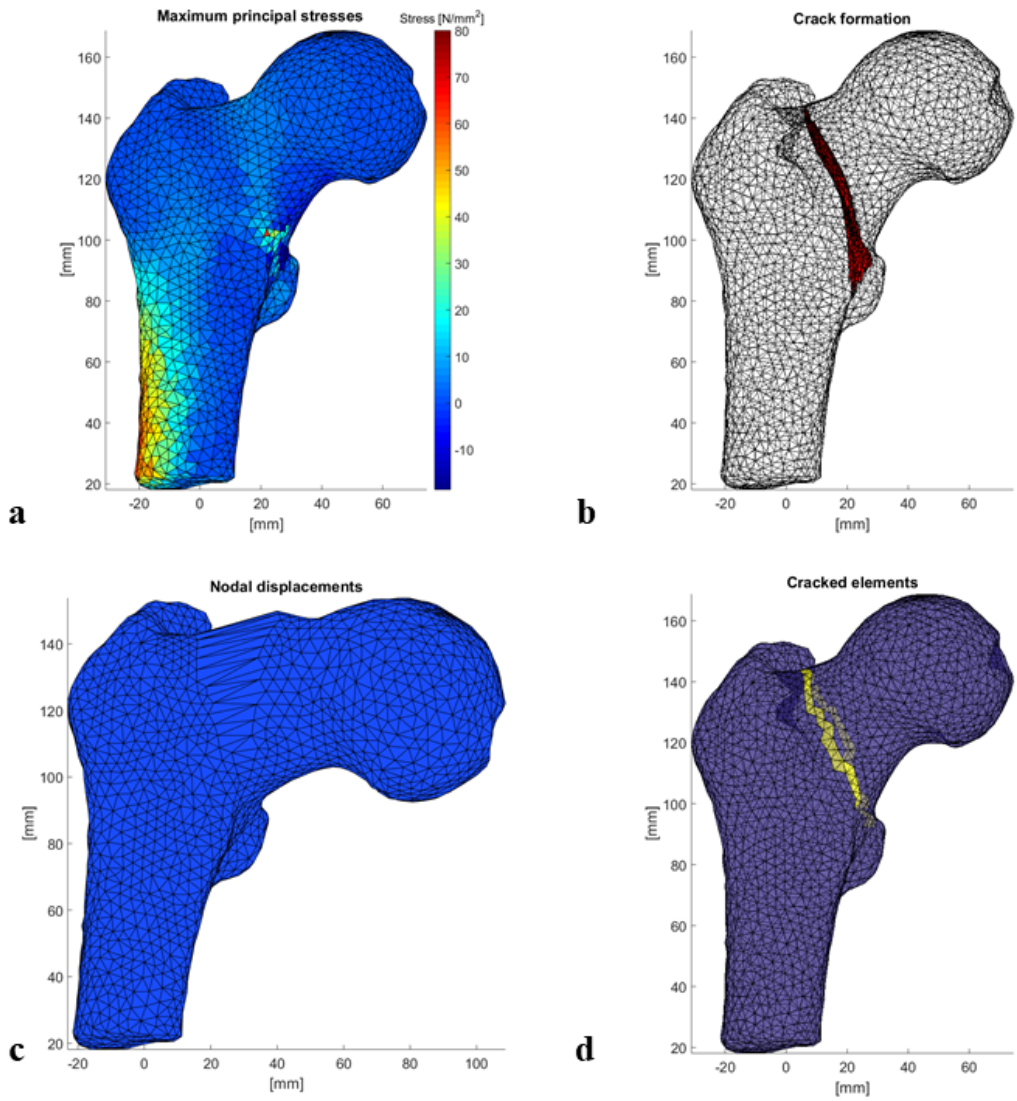

Figure 4.7: Sample 1, 4 materials (homogeneous), (a) Maximum principal stresses, (b) Crack formation, (c) Nodal displacements (enhanced by a factor 5), (d) Elements cracked

4.2.2 Cohesive strength

The results from varying values of the cohesive strength can be seen in figure 4.8 below:

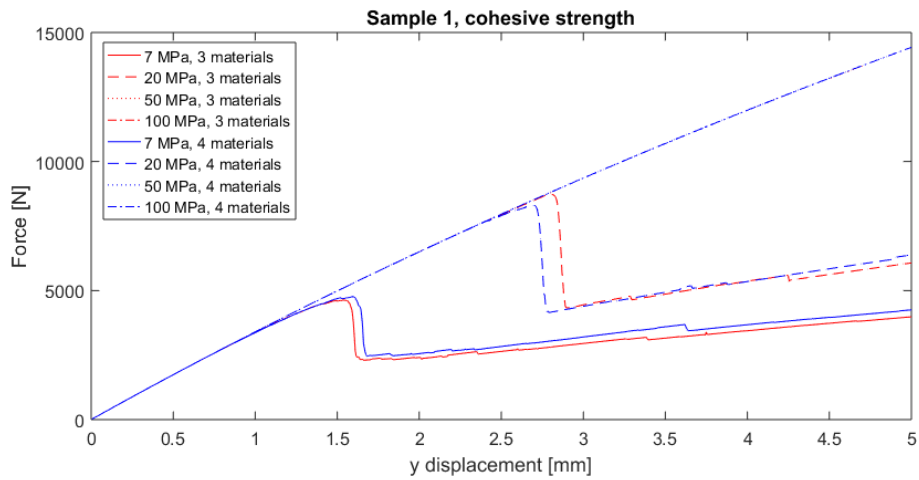

Figure 4.8: Force-displacement curve for varying values of cohesive strength, sample 1 (homogeneous models)

In table 4.2 below, the force and displacement for crack initiation and opening for different cohesive strengths are summarized. The force is recorded at the most superior nodes of the femoral head and the displacement is recorded at the control node used in the arc-length method, i.e. a node located lateral on the femoral head.

Table 4.2: Force and displacements at crack initiation and crack opening for varying cohesive strength, sample 1 (homogeneous models)

(a) 3 materials

$\sigma_{max}[MPa]$	**Crack initiation**		**Crack opening**	
	Force [N]	**Disp. [mm]**	**Force [N]**	**Disp. [mm]**
7	1 619	0.47	4 637	1.54
20	4 469	1.34	8 786	2.81
50	10 396	3.39	-	-
100	-	-	-	-

(b) 4 materials

$\sigma_{max}[MPa]$	**Crack initiation**		**Crack opening**	
	Force [N]	**Disp. [mm]**	**Force [N]**	**Disp. [mm]**
7	1 534	0.44	4 766	1.60
20	4 217	1.26	8 339	2.70
50	9 888	3.20	-	-
100	-	-	-	-

As shown in table 4.2, no crack opening occurred for the two highest values of cohesive strength (50 and 100 MPa) and for the highest (100 MPa), no crack occurred at all at the current displacement applied. For more details, see section 5.2.2. The onset of the crack paths for the homogeneous models with varying cohesive strength looked similar for all values. A more accurate analysis was not possible due to the short (or non-existing) crack paths which occurred for the models with higher values of cohesive strength. To quantify the variation of crack initiation point, the crack initiation point for the lowest value of cohesive strength (i.e. 7 MPa) was used as reference and the distance from the crack initiation point for a cohesive strength 20 and 50 MPa was calculated.

The crack initiation point varied as a maximum of 3.23 mm for the models with three materials (between the models with 7 and 20 MPa) and 0.0047 mm for the models with and four materials (between the models with 7 and 50 MPa). The maximum difference in crack initiation point between the models of three and four materials was calculated

as the difference of the mean of each coordinate, resulting in a maximum difference in x-coordinate, with a value of 1.82 mm. For more details, see Appendix, table 7.1. The crack path did not noticeably change from the one presented for the baseline model, figure 4.5, and are therefore not shown here.

4.2.3 Stiffness

Homogeneous model

The results from the homogeneous model of sample 1 with varying values of the Young's modulus (E) can be seen in figure 4.9 below:

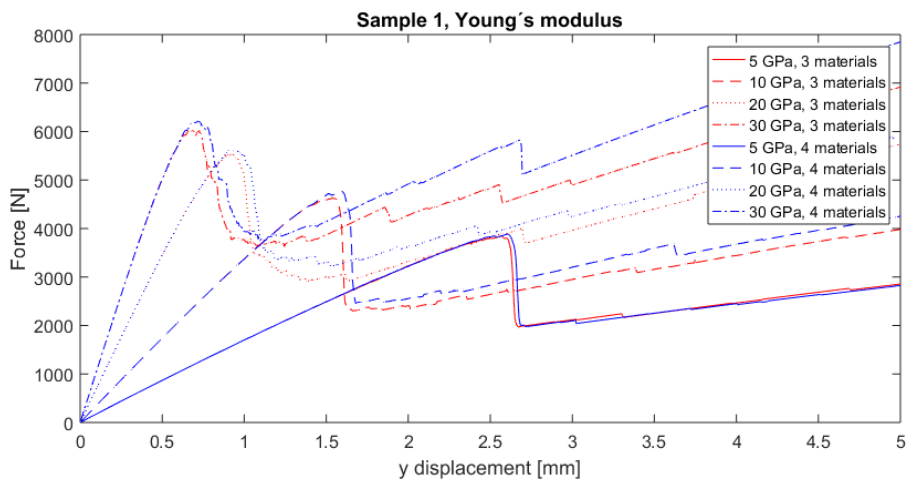

Figure 4.9: Force-displacement curve for varying values of Young's modulus, sample 1 (homogeneous model)

Table 4.3: Force and displacements at crack initiation and crack opening for varying Young's modulus, sample 1 (homogeneous model)

(a) 3 materials

$E[GPa]$	**Crack initiation**		**Crack opening**	
	Force [N]	**Disp. [mm]**	**Force [N]**	**Disp. [mm]**
5	1 585	0.93	3 840	2.57
10	1 619	0.47	4 637	1.54
20	1 654	0.24	5 538	0.93
30	1 643	0.16	6 035	0.67

(b) 4 materials

$E[GPa]$	**Crack initiation**		**Crack opening**	
	Force [N]	**Disp. [mm]**	**Force [N]**	**Disp. [mm]**
5	1 495	0.88	3 883	2.60
10	1 534	0.44	4 766	1.60
20	1 550	0.22	5 641	0.92
30	1 537	0.15	6 213	0.72

The crack path of the homogeneous models did not change noticeably between neither the models with three and four materials, nor with varying modulus compared to the models with baseline material values (figure 4.5). The difference in crack initiation point was calculated in the same way as described in the end of section 4.2.2, with the crack initiation point from the model with the lowest value of Young's modulus (i.e. 5 GPa) as reference point. In the homogeneous model with three materials the crack initiation point varied at a maximum with 3.23 mm (between the models with 5 and 10 GPa). For the model with four materials, the corresponding value was 0.0008 mm (between the models with 5, 20 and 30 GPa).

The maximum difference in crack initiation point between the models of three and four materials was calculated as the difference of the mean of each coordinate, resulting in a maximum difference in x-coordinate, with a value of 1.90 mm. For more details, see Appendix, table 7.2.

Heterogeneous model

The results from the heterogeneous model of sample 1 with the material parameters of the cortical bone tissue fixed at baseline values (Young's modulus = 10 GPa) and with varying values of the trabecular Young's modulus (E) can be seen in figure 4.10 below:

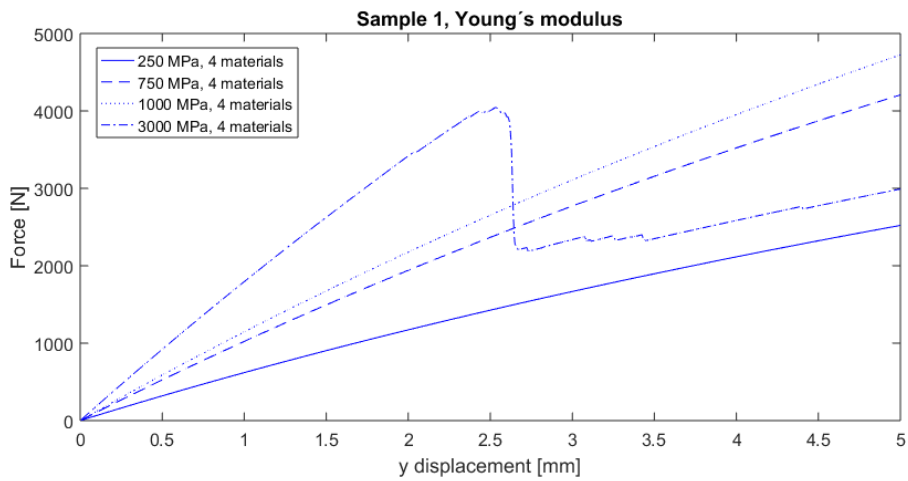

Figure 4.10: Force-displacement curve for varying values of Young's modulus of the trabecular bone (Young's modulus for cortical bone fixed at 10 GPa), sample 1 (heterogeneous model)

The values of force and displacement at crack initiation can also be seen in table 4.4 below. Only the model with a trabecular Young's modulus of 3 000 MPa reached a crack opening at a force of 4 044 N and the displacement 2.54 mm. This was due to the softer trabecular material in the other models (250, 750 and 1000 MPa), resulting in flatter slopes of the force-displacement curves. To reach the fracture energy needed to achieve a crack opening, the displacement needs to be higher. In the current case, the maximum displacement possible to apply was 5 mm, i.e. not enough to achieve a crack opening. For more details, see section 5.2.3.

Table 4.4: Force and displacements at crack initiation for varying Young's modulus, sample 1 (heterogeneous model)

E $[MPa]$	**Force [N]**	**Displacement [mm]**
250	1 306	2.26
750	1 379	1.38
1 000	1 403	1.24
3 000	1 537	0.85

In figure 4.11, the nodal displacements for varying modulus of the trabecular bone can be visualized. The results come from the heterogeneous model of sample 1 with four materials. For clarifying purposes, the nodal displacements have been enhanced by a factor 5.

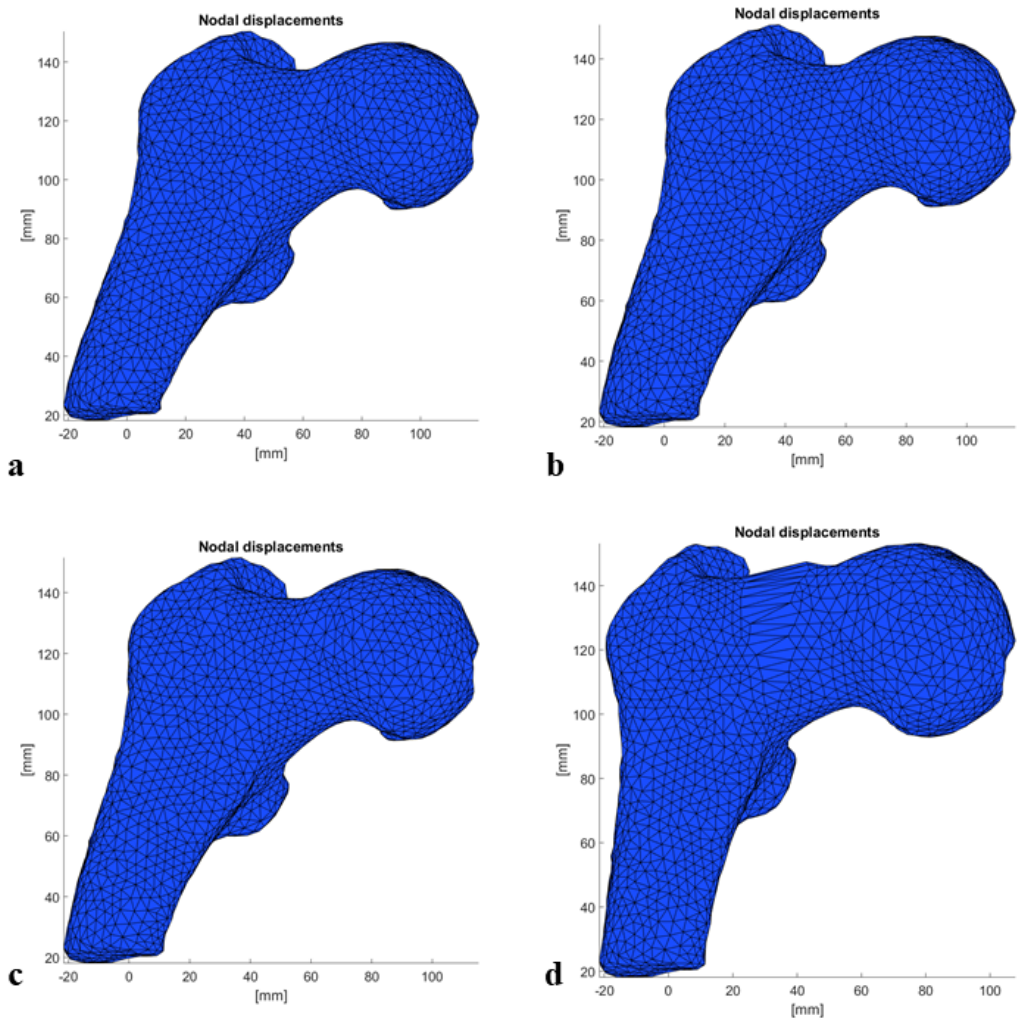

Figure 4.11: Nodal displacements (enhanced by a factor 5) at an applied displacement of 5 mm, sample 1 (heterogeneous model), (a) $E = 250MPa$, (b) $E = 750MPa$, (c) $E = 1000MPa$, (d) $E = 3000MPa$

The crack paths for all the heterogeneous models exhibited a similar behavior as the baseline model, figure 4.5, and are not therefore not shown here. Although the crack had propagated further in the model with the highest modulus compared to the lower, the onset of the cracks looked alike. For the crack initiation point, again calculated in the same way as in section 4.2.2, with the crack initiation point from the model with the lowest value of Young's modulus (i.e. 250 MPa) as reference

point, the maximum difference was 0.0036 mm (between the models with 250 and 3000 MPa). For more details, see Appendix, table 7.3.

Chapter 5

Discussion

The aim of this study was to use PUFEM in order to create subject-specific fracture predictions of the human femur. In order to reach this aim, a subject-specific FE modeling method was combined with a PUFEM-based code that worked on homogeneous material. A convergence study was performed in order to find a suitable step-size in the solution method, as well as a material parameters study to confirm the accurate mechanical response of the models. The goal of the material parameter study was also to assess the influence in terms of fracture initiation point and pathway.

At the current stage, several models have been produced and tested, homogeneous models of three and four materials modeled with the same material parameters, and heterogeneous models of four materials with the cortical and trabecular bone being modeled with different material parameters. With these models, it was possible to calculate crack initiation and path as well as obtaining the stress distribution and nodal displacements.

5.1 Convergence study

The purpose of the convergence study was to find the appropriate step-size to use in the solutions method. This was made by recording crack initiation point, force and displacement at crack initiation as well as at crack opening. When no significant changes were detected for decreasing step-size, the model had converged.

The results from the convergence study, figure 4.1, show a clear convergence for the model consisting of three materials (decreasing step-size corresponding to decreasing differences in crack initiation point). For the model consisting of four materials, the results are not as clear. An increase in distance occurred between the step-sizes 0.1 and 0.05 mm as well as between 0.001 and 0.0005 mm. However, the differences between the step-sizes of 0.005 and 0.0005 mm are still noticeably small.

The results from the convergence study in terms of force versus varying step-sizes, figure 4.4, showed very low variation in terms of force and displacement for crack initiation (for displacement versus varying step-sizes, see Appendix, figure 7.1). The values of the maximum force and displacement seem to demonstrate a slight decrease with decreasing step-sizes. The values appear to have stabilized for the step-sizes 0.005, 0.001 and 0.0005 mm, which correlates well with the results from the crack initiation coordinates. Based on these results, three options of step-sizes remained; 0.005, 0.001 and 0.0005 mm. Because of the small differences, and in order to save computational power and time, a step-size of 0.005 mm was used.

The purpose of testing homogeneous models with both three and four materials was to test the stability of the fracture initiation criterion and two-step algorithm. The subroutines obtained from [2], which implemented these features in the FEAP-software, where not adapted for handling crack propagation through multiple materials. This is a feature implemented during this project and therefore need to be thoroughly tested and evaluated. The convergence study indicated a low, but nevertheless, an existing variation between the models consisting of three and four materials. The homogeneous models consisting of three and four materials are modeled with the exact same material parameters, and should therefore exhibit identical behavior. Even-so, a slight difference can be seen between the two. These differences are most likely due to the method of averaging in the Rankine criterion as described in section 2.5.2. If this fracture initiation criterion is used in a model consisting of more than one material, there is a material line separating the different materials. If the element which is investigated is located in proximity of this material limit, the averaging process changes. If the sphere surrounding the element crosses a material line, the averaging only includes those elements in the sphere, which belong to the same

material as the element in question (see figure 5.1 (b)).

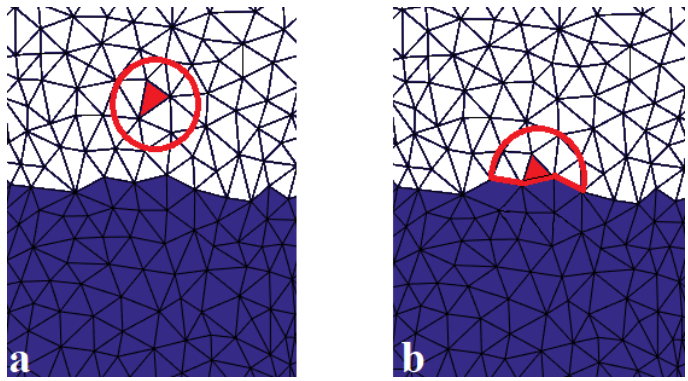

Figure 5.1: Averaging for the Rankine criterion in 2D over one (a) and two (b) materials

If changes were made to the subroutines describing the averaging method, so the averaging would be made independently of the number of materials, the models are expected to behave alike.

A mesh convergence study was originally planned in order to test the appropriate mesh-size. Unfortunately, certain limitations in the subroutines which were used to implement the PUFEM in the FEAP software, made it impossible to perform simulations with meshes containing more than 50 000 elements. This meant that simulations were limited to quite coarse meshes for each bone sample, which each consisted of less than 50 000 elements. To avoid the high number of elements which would be the result in a refined mesh, the possibility to make local refinements was also evaluated. By performing a local refinement of the femoral neck and an enlargement of the elements in the femoral shaft, head and throchanter region, a mesh with less than 50 000 elements was achieved. However, the larger elements made the quality of the mesh poor, and some of the details in the segmentation was lost. If no limitations in mesh-sizes were present, several different sizes could be evaluated. As in the case of step-sizes, when no significant changes in results would be detectable, the model would have converged, and a mesh-size could be selected. An ongoing collaboration with T.C. Gasser, is currently investigating the possibility to perform simulations with larger meshes.

5.2 Material parameter study

5.2.1 Baseline model

The results from the simulations performed on sample 1, homogeneous model with four materials are shown in figure 4.5, 4.6 and 4.7. In figure 4.5 it can be noted how the crack propagates through the femoral neck and in figure 4.6, how a stress concentration follows the crack tip. In figure 4.6 a larger stress concentration can also be noted at the femoral shaft, proving the purpose of the material line introduces in the mesh as described in section 3.4.2. Without these lines, the crack formation would take place at the lateral femoral shaft instead of the femoral neck.

5.2.2 Cohesive strength

By increasing the cohesive strength in the different simulations, the expected mechanical responses of the models are obtained. With increasing cohesive strength, the values of force and displacement for crack initiation and crack opening increased accordingly (see figure 4.8 and table 4.2). The results showed similar behavior for the models with three and four materials, with a slight difference. Again, this difference can be caused by the different methods of averaging as described above. For a cohesive strength of 50 and 100 MPa, neither of the models showed a clear drop in force as a result of a crack opening. The reason is that due to limitations in the implemented subroutines, it is only possible to simulate 1 000 steps in a simulation. For the chosen step-size of 0.005 mm, that is equivalent to a maximum displacement of 5 mm. This means that if a longer simulation was possible, the models with the higher cohesive strength (50 and 100 MPa) would eventually crack as well.

For varying values of cohesive strength, a small variation in crack initiation point was obtained. For the models consisting of three materials, the maximum difference was 3.2 mm (between the models with a cohesive strength of 7 and 20 MPa), and for the model with four materials it was 0.0047 mm (between the models with a cohesive strength of 7 and 50 MPa). The largest difference in crack initiation point between the models were 1.8 mm. These differences can be considered quite insignificant since the length of *one element* is approximately 3 mm.

5.2.3 Stiffness

By increasing the values of the Young's modulus for all materials in the homogeneous models (see figure 4.9 and table 4.3), the expected behavior of the model in terms of mechanical response was obtained. For increasing values of Young's modulus, the maximum force increased accordingly and the displacement at the same point decreased. The force needed for crack initiation was more or less the same for all values, while the displacement needed decreased for increasing values of the modulus. The fact that the crack initiation force remained constant for varying stiffness conforms well will the fracture initiation criteria which is based on stress. The cohesive strength is basically a threshold which determines *when* the crack will initiate, and since the cohesive strength remained the same in all models tested in this section, the force needed for crack initiation should have remained the same. The reason for the decreasing displacement needed can be explained by the fracture energy. The fracture energy is defined as the area under the force-displacement curve and with a steeper slope (a stiffer material), less displacement is needed in order to reach the same area as for a flatter slope (a softer material).

A small variation in terms of crack initiation point was also seen with varying Young's modulus. The largest difference for the models consisting of three materials, was 3.23 mm (between the models with a Young's modulus of 5 and 10 GPa), and 0.0008 mm for the model with four materials (between the models with a Young's modulus of 5, 20 and 30 GPa). The largest difference in crack initiation point between the models of three and four materials was 1.90 mm.

The expected mechanical response was also obtained for the heterogeneous model with varying values of the Young's modulus. The force needed for crack initiation remained similar with increasing values, while the displacement decreased. However, for the models with a modulus of 250, 750 and 1000 MPa, no crack opening occurred, i.e. no maximum force and displacement at that point could be registered. This means that the maximum principal stress did exceed the cohesive strength (σ_{max}), but the energy did not reach the fracture energy ($\mathcal{G}_c$), as described above. Important to note is that due to limitations in the implemented subroutines, it is only possible to simulate 1 000 steps in a simulation. For the chosen step-size of 0.005 mm, that is equivalent to

a maximum displacement of 5 mm. If the possibility to perform longer simulation existed, the models with the lower modulus would eventually crack as well. In addition, to obtain the energy level is at the current time also not possible. In order to obtain more insight into the behavior of the models and how the crack is progressing, this would be a feature which would be desirable in the future.

In figure 4.11, the nodal displacements of the heterogeneous models can be seen. With a "softer" material, the material did not crack from the displacement applied on the model (5 mm), but deformed. The lower the modulus, the larger are the displacements, indicating a deformation of the bone (4.11 (a, b, c)). However, all models would eventually crack if a sufficiently large displacement was applied, as mentioned above. In the model with a modulus of 3000 MPa, figure 4.11 (d), where a crack did occur, a "prolongation" of the cracked elements can instead be seen and no significant bending. Even though the bone is modeled heterogeneous, with varying values of the stiffness, the cohesive strength is the same. A more accurate representation might be to have a different cohesive strength for different stiffnesses.

Regarding the crack initiation point for the heterogeneous model, the largest change for varying values of Young's modulus was 0.0036 mm. The result that the crack initiation point is not affected by softening the trabecular bone, indicated that the cortical bone is responsible for carrying the majority of the load applied. These results correspond well with existing results from literature which indicated the less significant impact on bone strength of trabecular bone [34, 35]. The overall conclusion from the material parameter study is that the crack initiation point seem to vary little with varying values of the material parameters chosen in this project (cohesive strength and stiffness). Neither did the crack path seem to be much influenced by these variation. However, in some cases, the crack did not propagate far, making it hard to compare with longer pathways. The conclusion that the crack initiation point and path are not significantly influenced by varying the material parameters chosen in this project, indicates that these are more likely to be the results of the current boundary conditions and the bone geometry. It was also noted that the models consisting of four materials showed less variation than the models consisting of three. This lesser variation might again been caused by the difference averaging methods

described in section 2.5.2 and 5.1. For the models with four materials, the averaging will take place at a material limit, thus will the averaging be made over a smaller volume than it would in the model with three materials. With a smaller volume to average over, the variation in maximum principal stress between the elements in that area could be expected to be smaller.

5.3 Comparison with experimental data

In order to validate the results obtained in this project, a comparison with the experimentally obtained crack path [1] and the crack initiation point from the numerical models [8] was made. Only small variations in crack formation could be seen between the models, so for this comparison, sample 1 with four materials and baseline material parameters was used.

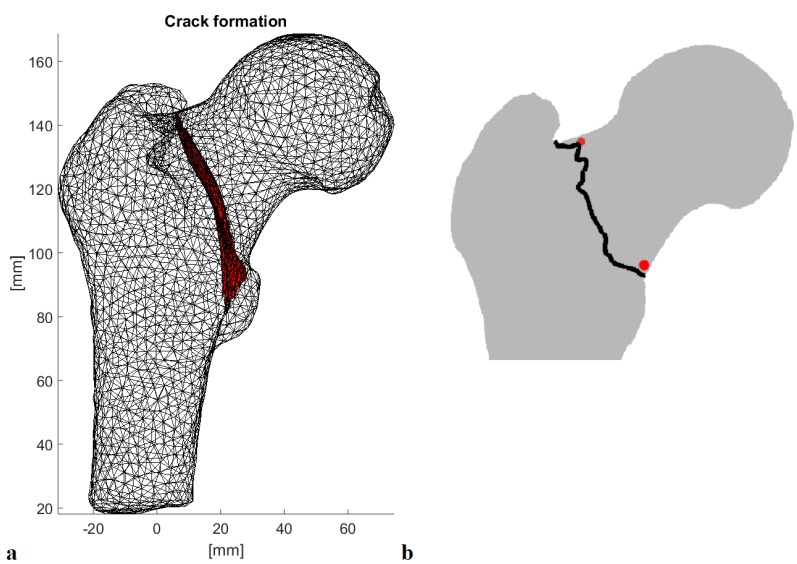

Figure 5.2: (a) Crack propagation, sample 1 with 4 materials, baseline material parameters (b) Experimentally obtained crack path (black) [1] and crack initiation from numerical models in [8] (red). Reprinted with permission from Elsevier

Through a visual comparison, both the crack path and crack ini-

tiation points seem to exhibit similar patterns. The crack path from the numerical models made in this project exhibits a straighter behavior than the experimentally obtained one. A reason for this could be the lack of micro-structural organization of the bone in the numerical model. Where it in the real femur would have been cavities, is in the present case modeled as solid, homogeneous, matter. This makes it possible for a straight crack path to develop in the model, but not in the real femur. Another major contributor for the straight crack path is the corrector-step of the two-step algorithm used for tracking cracks. This step ensures for a smoother crack-surface.

The two red marks in figure 5.2 (b) indicate the starting points for the crack resulting from the numerical models in [8]. The top element cracked as a result of tension, the lower one of compression. In the present work, an element can only crack due to tension according to the cohesive crack concept, and the option to crack as a result of compression is not implemented.

A comparison of the the force-displacement curves from the model based on sample 1 (homogeneous model with four materials and baseline material parameters) with the results from [1] (see figure 5.3) was made. From this, it can be noted that the maximum force, and the displacement at this force, are significantly smaller for the first one (4 766 N and 1.6 mm vs. 7 856 N and approximately 6.1 mm).

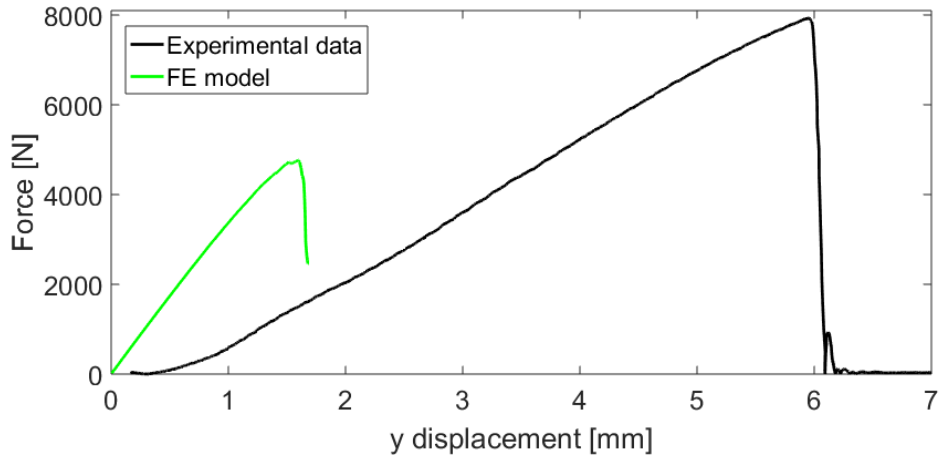

Figure 5.3: Force-displacement curve from sample 1, homogeneous model, 4 materials, baseline material parameters (green), force-displacement curve from [1] (black)

The much smaller values obtained in this project could probably be explained by the fact that the materials parameters chosen for the models are not yet adjusted according to those of the actual bone samples. For example, both the elastic modulus (E) and the cohesive strength (σ_{max}) are probably underestimated when comparing to data from literature [32, 29]. Of the models produced in this project, the one which exhibited the best fit to the experimental data in terms of stiffness was the heterogeneous model of sample 1 with a trabecular Young's modulus of 3 000 MPa (cortical Young's modulus 10 GPa). This force-displacement plot can be compared to the experimental data in figure 5.4 below.

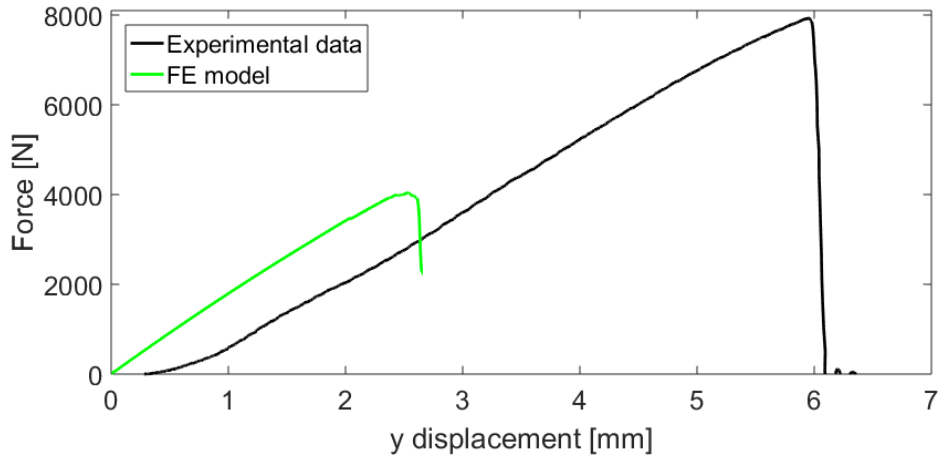

Figure 5.4: Force-displacement curve from sample 1, heterogeneous model, 4 materials, trabecular Young's modulus 3 000 MPa (green), force-displacement curve from [1] (black)

As seen in figure 5.4, the slope of the curves, i.e. the stiffness, are much more similar. However, a large difference in crack opening can still be seen, which would make the next step to adjust the values of the cohesive strength. In figure 5.5 below, the cohesive strength in the model shown in 5.4 has been increased to a value of 20 MPa, resulting in the best fit to the experimental data so far.

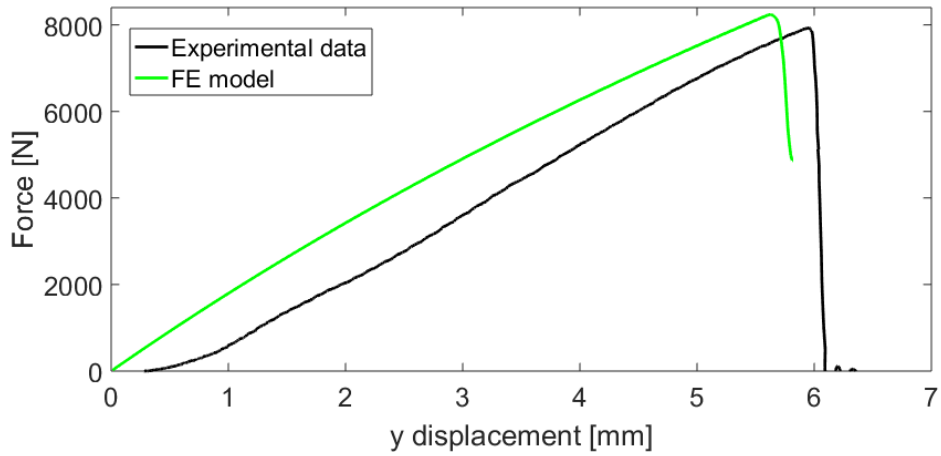

Figure 5.5: Force-displacement curve from sample 1, heterogeneous model, 4 materials, trabecular Young's modulus 3 000 MPa, cohesive strength 20 MPa (green), force-displacement curve from [1] (black)

Another reason for the differences between experiment and FE-models could be the different boundary conditions. Although the boundary conditions assigned to the models aimed at simulate those in the experiments, the epoxy pot is missing from the models. This could have contributed to an overall higher stiffness, making its absence a contributor to the lower values in the models.

5.4 Limitations and future work

As a future step for this project, it would be appropriate to develop a finite element model with a more accurate representation of the material parameters. Although the current solution of modeling the bone with two different materials, cortical and trabecular bone, is an improvement when comparing to homogeneous models, a more detailed mapping of the actual material parameters could be beneficial. The software Bonemat [36] allows for a direct mapping of the elastic properties to each finite element by using the density from CT-images. The output is a finite element mesh containing the material properties in each element which can be used as input in various finite element programs. However, at the current time, to combine Bonemat with the implemented subroutines in FEAP, is not possible. Due to the different averaging method

which occurs when a material line is present, this would become very cumbersome since each element would be defined as a new material after the use of Bonemat. From the author's point of view, there are two options available: to define all elements as one material model, but to read in the element-specific material parameters from a separate file, or to change the averaging method. By altering the subroutines to allow averaging over multiple material models, the Bonemat software could most probably be used.

Something which could be seen as a limitation in the current models is that the marrow canal is not considered. For a more realistic model, the marrow canal should be modeled with a significantly lower elastic modulus than in the present case. However, this limitation is expected to have a minor impact on the results in comparison to the experimental data provided in the project due to the mechanical setup. The part of the femur which would contain the marrow canal, i.e. the distal shaft, is in the mechanical tests of [1] fixed in the epoxy-pot, and would therefore be expected to "appear" stiffer.

This finite element model could, as mentioned above, be considered a more realistic representation of human bone than some existing models, due to the separate modeling of cortical and trabecular bone. However, the current model does not consider the actual trabeculae, the honeycomb shape. A further development of the model could therefore be an even more thorough segmentation, where this is included. Important to note is however that this would require micro-CT-images and a more powerful mesh generation program. Although this could be a solution for obtaining a more accurate representation of bone, the method of using micro-CT-images would not be applicable if the fracture prediction were to be used on living human beings. The reason for this is that micro-CT-images require a much higher radiation dose than what would be allowed in regions in the proximity of the reproductive organs, such as the region where the proximal femur is located. However, if the purpose of the fracture predictions would be for modeling only, the use of micro-CT-images might be appropriate. Although, studies have shown that the trabecular part of the bone are less significant in predictions of bone strength [34, 35], indicating that modeling of the trabecular micro-structure would be unnecessary.

In order to test the stability of the model, one option could be to try different loading directions. Large fluctuations in e.g. crack initiation location for small changes in loading directions would indicate an instable model and adjustments would need to be made. Another option would also be to test different boundary conditions in order to confirm or contradict the assumption that the crack initiation point and path is more influenced by those (and bone geometry) than by the material parameters.

5.5 Ethical aspects

In this project, CT-images from two human femurs were used. Both bone samples were previously used in the study of [1] and obtained through an ethically approved protocol (ethical permission by National Authority for Medicolegal Affairs 5783/2004/044/07). By re-using these CT-images in an anonomyzed fashion, no new samples were needed and no personal data were handled.

At the current stage, the models are not sophisticated enough to be implemented in clinics as a tool to predict fractures, but they have potential to be in the future. One can reflect on whether information about this is beneficial or not. To get information as a patient that a fracture may occur in a specific location and at a certain load may not be helpful. However, if this information can be used to predict generalized fracture risk, then the patient may be treated for such with e.g. bisphosphonates or new bone boosting drugs. Also increased physical activity, e.g. physical therapy, can lead to better muscle control and thereby a reduced risk of falling. All together this would be highly beneficial to the patient. Another question to consider if the models would be implemented in clinics would be to determine who will receive this assessment. To perform this type of fracture risk assessment, CT-images are currently needed which would mean exposure to radiation for the patient. However, the Biomechanics group in Lund are working to enable performing these simulations on 2D DXA images, which would greatly reduce the radiation. Still, exposure to radiation should be avoided if possible and the assessment would therefore be more appropriate to only offer to people in a certain age or risk group.

Chapter 6

Conclusions

The Finite Element models produced in this project are subject-specific, with both three and four materials modeled homogeneous and heterogeneous, and are able to accurately predict the crack initiation point as well as crack path when compared to experimental data.

The conclusion are that the models

- exhibit the expected results in terms of mechanical response with varying material parameters.
- show that the crack initiation point and crack path are not significantly influenced by varying material parameters, thus indicating that these are more likely the results of the currently prescribed boundary conditions and bone geometry.
- exhibit more variation in terms of crack initiation in models with three materials than four. This indicates that the models with four materials, modeled heterogeneously should be used for future modeling in order to obtain low variation and a more realistic representation of bone.

Bibliography

[1] Lorenzo Grassi, Sami P. Väänänen, Saber Amin Yavari, Jukka S. Jurvelin, Harrie Weinans, Matti Ristinmaa, Amir A. Zadpoor, and Hanna Isaksson. Full-Field Strain Measurement During Mechanical Testing of the Human Femur at Physiologically Relevant Strain Rates. *Journal of Biomechanical Engineering*, 136(11):111010, 2014.

[2] T. Christian Gasser and Gerhard A. Holzapfel. A numerical framework to model 3-D fracture in bone tissue with application to failure of the proximal femur. *Solid Mechanics and its Applications*, 5:199–211, 2007.

[3] B Gullberg, O Johnell, and J A Kanis. World-wide Projections for Hip Fracture. *Osteoporos Int*, 44(1997):407–413, 1997.

[4] Frederic H. Martini and Edwin F. Bartholomew. *Essentials of human anatomy & physiology*. Pearson Education, Inc., Glenview, IL, USA, sixth edition, 2015.

[5] Vinay Kumar, Abul K. Abbas, Nelson Fausto, and Richard N. Mitchell. *Robbins basic pathology*. Saunders, Elsevier Inc, Philadelphia, USA, eighth edition, 2007.

[6] A. Svedbom, E. Hernlund, M. Ivergård, J. Compston, C. Cooper, J. Stenmark, E. V. McCloskey, B. Jönsson, and J. A. Kanis. Osteoporosis in the European Union: A compendium of country-specific reports. *Archives of Osteoporosis*, 8(1-2), 2013.

[7] Nelson B. Watts, Bruce Ettinger, and Meryl S. LeBoff. FRAX facts. *Journal of Bone and Mineral Research*, 24(6):975–979, 2009.

[8] Lorenzo Grassi, Sami P. Väänänen, Matti Ristinmaa, Jukka S. Jurvelin, and Hanna Isaksson. How accurately can subject-specific finite element models predict strains and strength of human femora? Investigation using full-field measurements. *Journal of Biomechanics*, 49(5):802–806, 2016.

[9] Thomas C. Gasser and Gerhard A. Holzapfel. 3D Crack propagation in unreinforced concrete. A two-step algorithm for tracking 3D crack paths. *Computer Methods in Applied Mechanics and Engineering*, 195(37-40):5198–5219, 2006.

[10] T.D Moran. Visual Histology - Histology Text Atlas Book, Chapter 6: Bone.

[11] John A. Kanis. Diagnosis of osteoporosis and assessment of fracture risk. *Lancet*, 359(9321):1929–1936, 2002.

[12] WHO. *World Health Organization Scientific Group on the Assessment of Osteoporosis At Primary Health*. 2004.

[13] Lorenzo Grassi. *Femoral strength prediction using finite element models*. PhD thesis, Lund University, 2016.

[14] C. H. Turner and D. B. Burr. Basic biomechanical measurements of bone: A tutorial. *Bone*, 14(4):595–608, 1993.

[15] Amnon Sharir, Meir Max Barak, and Ron Shahar. Whole bone mechanics and mechanical testing. *Veterinary Journal*, 177(1):8–17, 2008.

[16] L Cristofolini, M Viceconti, A Cappello, and A Toni. MECHANICAL VALIDATION OF WHOLE BONE COMPOSITE FEMUR MODELS. *Journal of Biomechanics*, 29(4):525–535, 1996.

[17] Olli Leppänen, Harri Sievänen, Jarkko Jokihaara, Ilari Pajamäki, and Teppo L N Järvinen. Three-point bending of rat femur in the mediolateral direction: Introduction and validation of a novel biomechanical testing protocol. *Journal of Bone and Mineral Research*, 21(8):1231–1237, 2006.

[18] L. Grassi, E. Schileo, F. Taddei, L. Zani, M. Juszczyk, L. Cristofolini, and M. Viceconti. Accuracy of finite element predictions in sideways load configurations for the proximal human femur. *Journal of Biomechanics*, 45(2):394–399, 2012.

[19] Niels Ottosen and Hans Petersson. *Introduction to the Finite Element Method*. Pearson Education, Limited., Essex, Great Britain, 1992.

[20] Robert L Taylor and Sanjay Govindjee. FEAP - A Finite Element Analysis Program, User manual, 2017.

[21] E. J. Lotz, J. C. Cheal and W. C. Hayes. Fracture Prediction for the Proximal Femur Using Finite Element Models: Part I—Linear Analysis. *Journal of Biomechanics*, 113(4):353–360, 1991.

[22] J. M Melenk and I Babuskab. The partition of unity finite element method: Basic theory and applications. *Computer methods in applied mechanics and englneerlng*, (139):289–314, 1996.

[23] ABAQUS 6.12 Dassault Systèmes®. 10.7.1 Modeling discontinuities as an enriched feature using the extended finite element method.

[24] B. R. K. Blackman, H. Hadavinia, Anthony J. Kinloch, and J. G. Williams. The use of a cohesive zone model to study the fracture of fibre composites and adhesively-bonded joints. *International Journal of Fracture*, 119(1):25–46, 2003.

[25] T. Christian Gasser. Validation of 3D crack propagation in plain concrete. Part II: Computational modeling and predictions of the PCT3D test. *Computers and Concrete*, 4(1):67–82, 2007.

[26] S. Krenk. *Non-linear Modeling and Analysis of Solids and Structures*. Cambridge University Press, Cambridge, United Kingdom, 2009.

[27] G. M. Treece, K. E S Poole, and A. H. Gee. Imaging the femoral cortex: Thickness, density and mass from clinical CT. *Medical Image Analysis*, 16(5):952–965, 2012.

[28] Mechanics Structural Engineering, Materials, Department of Civil and Environmental Engineering, and Berkeley University of California. FEAP A Finite Element Analysis Program, 2017.

[29] Emer M. Feerick, Xiangyi Cheryl Liu, and Patrick McGarry. Anisotropic mode-dependent damage of cortical bone using the extended finite element method (XFEM). *Journal of the Mechanical Behavior of Biomedical Materials*, 20:77–89, 2013.

[30] Naiara Rodriguez-Florez, Alessandra Carriero, and Sandra J. Shefelbine. The use of XFEM to assess the influence of intra-cortical porosity on crack propagation. *Computer Methods in Biomechanics and Biomedical Engineering*, 20(4):385–392, 2017.

[31] Susan Mischinski and Ani Ural. Finite Element Modeling of Microcrack Growth in Cortical Bone. *Journal of Applied Mechanics*, 78(4):041016, 2011.

[32] Harun H. Bayraktar, Elise F. Morgan, Glen L. Niebur, Grayson E. Morris, Eric K. Wong, and Tony M. Keaveny. Comparison of the elastic and yield properties of human femoral trabecular and cortical bone tissue. *Journal of Biomechanics*, 37(1):27–35, 2004.

[33] Emil Fågelberg, Lorenzo Grassi, Per Aspenberg, and Hanna Isaksson. Surgical widening of a stress fracture decreases local strains sufficiently to enable healing in a computational model. *International Biomechanics*, 2(1):12–21, 2015.

[34] Janne E M Koivumäki, JérÔme Thevenot, Pasi Pulkkinen, Volker Kuhn, Thomas M. Link, Felix Eckstein, and Timo Jämsä. Cortical bone finite element models in the estimation of experimentally measured failure loads in the proximal femur. *Bone*, 51(4):737–740, 2012.

[35] Gerold Holzer, Gobert Von Skrbensky, Lukas A. Holzer, and Wolfgang Pichl. Hip fractures and the contribution of cortical versus trabecular bone to femoral neck strength. *Journal of Bone and Mineral Research*, 24(3):468–474, 2009.

[36] Insituto Ortopedico Rizzoli. Bonemat, 2015.

Appendix

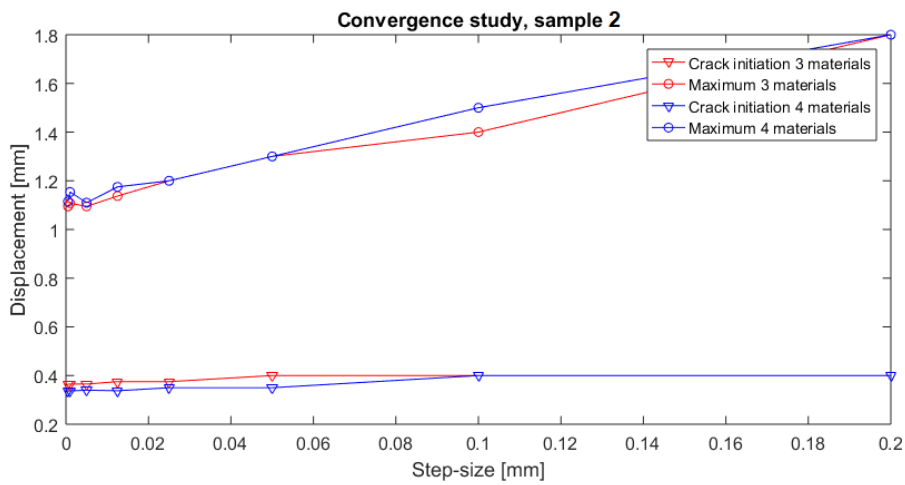

Figure 7.1: Results from convergence study, displacement vs. step-size, sample 2 (homogeneous models)

(a) 3 materials

$\sigma_{max}[MPa]$	**x**	**y**	**z**
7	8.97	144.52	-15.50
20	7.97	143.03	-18.19
50	8.97	144.53	-15.50
100	-	-	-

(b) 4 materials

$\sigma_{max}[MPa]$	**x**	**y**	**z**
7	6.82	142.78	-17.87
20	6.82	142.78	-17.87
50	6.82	142.78	-17.87
100	-	-	-

Table 7.1: Crack initiation point for varying cohesive strength, sample 1 (homogeneous models)

(a) 3 materials

E $[GPa]$	**x**	**y**	**z**
5	7.97	143.03	-18.19
10	8.97	144.52	-15.50
20	8.97	144.52	-15.50
30	8.97	144.52	-15.50

(b) 4 materials

E $[GPa]$	**x**	**y**	**z**
5	6.82	142.78	-17.87
10	6.82	142.78	-17.87
20	6.82	142.78	-17.87
30	6.82	142.78	-17.87

Table 7.2: Crack initiation point for varying Young's modulus, sample 1 (homogeneous models)

E $[MPa]$	**x**	**y**	**z**
250	9.69	143.79	-16.12
750	9.69	143.79	-16.12
1000	9.69	143.79	-16.12
3000	9.69	143.80	-16.12

Table 7.3: Crack initiation point for varying Young's modulus, sample 1 (heterogeneous models)